Theses and Dissertations

8-2014

Multiple Reference Impact Testing of Bridges Using a Network of Low-Cost Dynamic Exciters

James David Lindsey
University of Arkansas, Fayetteville

Multiple Reference Impact Testing of Bridges Using a Network of Low-Cost Dynamic Exciters

Multiple Reference Impact Testing of Bridges Using a Network of Low-Cost Dynamic Exciters

A thesis submitted in partial fulfillment
of the requirements for the degree of
Master of Science in Engineering

By

James David Lindsey
North Carolina A&T State University
Bachelor of Science in Civil Engineering, 2012

August 2014
University of Arkansas

This thesis is approved for recommendation to the Graduate Council.

_____
Dr. Kirk Grimmelsman
Thesis Director

_____   _____
Dr. Micah Hale   Dr. R. Panneer Selvam
Committee Member   Committee Member

ABSTRACT

Multiple Reference Impact Testing (MRIT) is a form of Experimental Modal Analysis (EMA) that can be used to identify the dynamic properties of full-scale bridges. These dynamic properties include natural frequencies, mode shapes, damping ratios, modal scaling and modal flexibility. Since these system properties that are directly related to the mass and stiffness characteristics of a structure, impact test measurements can be used to quantitatively characterize condition of a structure. Over time, changes in the properties can be monitored and evaluated as indicators of damage or deterioration. Instrumented hammers and drop masses are typically used to perform MRIT by providing impulsive dynamic excitation to a structure. The corresponding vibration responses are measured using accelerometers. This approach has a number of practical and experimental shortcomings, including that the testing is time consuming, the impulsive forces produced can be variable, it interferes with the normal operation of the structure, and it is not suitable for continuous monitoring applications.

The research herein, evaluates a new method for performing MRIT testing by comparing it to a conventional MRIT testing method. A small-scale and inexpensive excitation device is roved amongst spatially distributed input points to provide dynamic excitation. The excitation device can be inexpensively deployed in large numbers on a structure and programmed to produce a sequence of impulsive dynamic forces. This approach has several important advantages over conventional MRIT testing. For instance, total testing time is reduced, the impulsive forces produced are more repeatable, the testing can be accomplished without affecting the normal operation of the structure, and most importantly, it is amenable to long-term and continuous monitoring applications. The new MRIT approach is evaluated on both a large-scale laboratory model and full-scale bridge structure. The dynamic characterization results for both structures

are compared with those obtained by the conventional MRIT approach using instrumented impact hammers.

ACKNOWLEDGEMENTS

First and foremost I must thank God for allowing me to reach this point in my academic career and being there for me every step of the way.

Thanks to my advisor Dr. Kirk Grimmelsman who allowed me to work with him the past two years. I am very appreciative of his knowledge, drive and commitment to the field of structural engineering; more importantly, his patience with me. His creativity has inspired me beyond measure and allowed me to work diligently on this research. I wish you the best in Philadelphia. I know that you will continue to do an outstanding job.

I would like to thank Dr. Micah Hale and Dr. R. Panneer Selvam for serving on my thesis committee, providing me with assistance, and being excellent professors.

None of this would have been possible without the inspiration, support and friendship of several fellow Civil Engineering students. Notably, Eric Fernstrom, Thomas Norris, Dawn Farver, Joseph Daniels and Korey Pough. Thank you for helping me with field and lab testing, technical questions, defense preparation and support in all manners.

Several long nights which seemed endless at times were spent working on this document, gathering data, and analyzing results. As expected, it is easy to have thoughts of giving up. Thank you to my beautiful girlfriend Ebony Rodgers for non-stop encouragement when every door seemed to close and every path seemed to be a dead end. Our conversations and your patience with me have gotten me to the finish line.

Last but not least, my parents Joe and Joyce Lindsey and my younger brother Nathan. Your kind thoughts, motivation, love and words in prayer have brought me a long way. There is nothing

like family and I know I have the best ever. From inspiring phone calls and text messages to packages in the mail that made my day, I can say that you all are the reason I have succeeded in completion of this thesis.

TABLE OF CONTENTS

CHAPTER ONE

INTRODUCTION

1.1 PROBLEM STATEMENT

The well-publicized status of the nation's aging and deteriorating transportation infrastructure assets has been a significant driving factor of research into more reliable methods for characterizing and evaluating their performance and condition. Structural Health Monitoring (SHM) and vibration based damage detection (VBDD) methods have been a particular focus in much of this research. Despite the considerable research that has been performed, these methods have yet to prove their full potential for improving the reliability and effectiveness of bridge management decisions. The technological barriers to measuring and monitoring the vibrations of bridge structures have been substantially minimized, but our understanding of the limitations and uncertainties associated with these experimental methods have not advanced at the same pace as the available technologies. Many researchers have studied the variations and uncertainty in the modal parameters identified by OMA due to the environment (temperature, humidity, solar radiation, etc.), but have not been able to measure and characterize the uncertainty due to the actual dynamic excitation. The uncertainty in the identified modal parameters, due to variations in the dynamic excitation from its assumed nature, limits the utility of the experimental results for many bridge assessment objectives. Numerous damage detection and identification algorithms have been developed for bridges that use measured vibrations or modal parameters as their starting point (Doebling et al., 1996); however, most of these algorithms have not yet proven to be very reliable outside of the laboratory (Brownjohn et al., 2011). Uncertainty in the modal parameters identified by OMA may be a significant contributing factor to this limitation.

With the release of the American Society of Civil Engineers (ASCE) Infrastructure Report in 2009, Americans learned that one in four of the nation's bridges is structurally deficient or functionally obsolete resulting in a grade of C. During this time, 72,868 (12.1%) bridges were labeled as structurally deficient and 89,024 (14.8%) were classified as functionally obsolete (2009 ASCE Report). Per the 2013 ASCE Infrastructure Report Card, one in nine of the nation's bridges is rated as structurally deficient or functionally obsolete. In addition, of the now 607,380 bridges, the average age is 42 years old. Since 2009, the grade has gone from a C to C+. This is due to a decrease in structurally deficient and obsolete bridges. On the other hand, the number of bridges closed to traffic has increased, which affects the grade as well. There is still much work to be done. The Federal Highway Association (FHWA) suggests that $20.5 billion be invested annually in order to prevent deficient bridge accumulation by 2028. Unfortunately, currently only $12.8 billion are spent annually (2013 ASCE Report Card).

While funds and expenses are an important factor when it comes to repairing our infrastructure, there is much more that must be considered. First, the deficiencies within each bridge must be noted and accounted for. However, the problem is that often the bridge inspection does not reveal all of the deficiencies. Most inspections are visual and at maximum are only done every two years. Second, it is important that the money invested to inspect and/or repair is used to perform tests that will yield the most useful results about damage detection.

1.2 MOTIVATION

Dynamic testing of bridges can be broken into two distinct, broad categories: Operational Modal Analysis (OMA) and Experimental Modal Analysis (EMA). In both methods of testing, the structure is assumed to be time invariant but the major difference is whether the excitation is

uncontrolled or controlled. OMA will yield more uncertainty because only the measured responses are used to find modal vectors, modal frequencies and damping ratios. The unmeasured and unknown input is caused by operating loads and ambient vibrations. OMA makes the general assumption that the excitation is stationary, broadband white noise that excites the given structure with the frequency band of interest. In contrast, EMA measures both the input and output responses. This ability to characterize and regulate the dynamic excitation is an advantage, because in addition to the modal parameters that OMA can identify, EMA can also evaluate modal scaling and flexibility (Fernstrom et. al, 2013).

The method of dynamic characterization performed during this research will be Multiple-Reference Impact Testing (MRIT). MRIT has been used to evaluate short to medium span bridges. As stated when describing EMA, MRIT can be utilized to identify the modal flexibility of a structure (Zhang & Moon, 2012). The flexibility of a structure is important when dealing with SHM. Naturally, a structure will become more flexible over its life span. However, if it is becoming more flexible at an alarming rate, precautions may need to be taken. This is something that cannot be determined via OMA. One drawback to MRIT is that a large amount of sensors must be employed on the structure at several locations. Another major issue with MRIT is exciting massive civil structures well above the noise level. Other issues that arise with MRIT are balancing leakage against poor signal-to-noise ratios and mistakenly exciting nonlinearities with the initial input force (Schwarz & Richardson, 1999).

The main objective of this research will be investigating a new method for dynamic characterization of bridges using MRIT. Multi-reference impact testing (MRIT) has been

employed to reliably and effectively determine modal parameters of a bridge, which can ultimately lead to defining the health of a bridge.

1.3 LITERATURE REVIEW OF IMPACT TESTING

In the late 1840s it was observed that materials behave far differently under static loads than they do when dynamic loads are applied. Between 1895 and 1922 several international and national codes and standards were developed in all engineering-related fields to perform various tests. Impact testing was included in some of these standards. The American Society for Testing and Materials (ASTM) and the International Association for Testing Materials were two organizations established to develop official testing methods (Stewart et al., 2000).

On December 15, 1967, the Silver Bridge (connecting Ohio and West Virginia), which crosses over the Ohio River, collapsed during rush hour and killed 46 people. As a result, the U.S. Congress developed the Federal Highway Act of 1968 and became law as the National Bridge Inspection Standard. Each state was required to establish an inspection organization, inspect no less than every two years, and set qualifications for individuals who would do the inspections. Prior to this disaster, states were only required to maintain and inspect bridges on the federal highway system. Furthermore, in states such as Virginia, underwater inspections were done by individuals who had "some" knowledge of structures (Coleman, 1996).

Within the past 30-40 years, the main push for bridge testing is due to a need for more reliable testing methods. As stated before the two broad categories to consider are Experimental Modal Analysis (EMA) and Operational Modal Analysis (OMA). Each of these can be further characterized by the following methods of testing: Single Input Single Output (SISO), Single Input Multiple Output (SIMO), and Multiple Input Multiple Output (MIMO). Multiple Input

Single Output (MISO) is also a form of testing that exists but more for theoretical purposes as opposed to practical. The research herein, Multiple Reference Impact Testing (MRIT), is considered to be SIMO because there are multiple reference points are impacted one at a time, but in sequence, while the accelerometers measure an output (Liao et al., 2012). Ambient vibration testing (AVT) assumes that all natural or unmeasured excitation is applied to the whole structure. This can be considered as using multiple inputs and multiple outputs. Forced Vibration Testing (FVT) is an EMA that uses input-output testing methods. There is a controlled and measured dynamic excitation. The EMA equivalent of MIMO is using tactile transducers at multiple input locations and measuring multiple outputs at once. When using AVT, natural frequencies, mode shapes and damping can be determined. Though more difficult to employ, FVT is superior, because it allows researchers to determine modal scaling and modal flexibility in addition to all of the properties that AVT can identify. Tests that involve measured input are limited to smaller bridges, whereas ambient tests are conducted on larger truss, suspension and cable-stayed bridges (Farrar et al., 1999). Brownjohn et al. compared, predicted and measured properties of the Humber Suspension Bridge using ambient vibration testing. Before actually testing this bridge, it was stated that mathematical models had been developed for various bridge types but are only reliable to a certain extent. Vertical, lateral, torsional, and longitudinal modes were obtained and compared to those computed from mathematical models. As far as vertical modes, those at lower frequencies were quite close when comparing measured results and predicted results. As the frequencies increased, the accuracy became smaller but was no higher than 5% error. It was found that the two-dimensional mathematical model can precisely predict frequencies and mode shapes of in-plane modes. The three dimensional model yielded good results for the torsional and vertical modes. They also stated that damping values are reliable but

are over-estimated and should be taken with caution. In addition, damping values decreased as frequencies increased and just one value could not be used for all modes (Brownjohn et al., 1987).

In the past, it has been proposed that changes in modal frequencies, mode shapes and stiffness generally indicate damage to a structure. However, uncertainty becomes a factor when high quality data acquisition is not used. Some typical limitations of modal testing include identifying a limited number of modes, measuring a single span on a multi-span bridge, testing reliability of mode shapes and frequencies, separating coupled modes, determining cause of damage, and lacking a system identification approach (Madhwesh & Aktan, 1992).

Impact hammers, linear mass shakers and eccentric mass shakers can all be reliable input devices for impact testing. However, often times this is not the case and there are many issues that come with using each one. Impact devices include sledge hammers, mini-hammers, and drop hammers, which are all manually operated. This type of impact device is most common because of its low cost, ease of portability, minimal need for equipment, ability to use on structures in its operational state, and use on moving systems. Researchers have collected modal analysis data by roving the hammer to different locations while leaving the input location fixed and vice versa. For MRIT, however, the only practical procedure is roving the hammer. Along with this procedure, comes the difficulty of impacting at certain angles for each impact point, which may not be physically possible (Fladung & Brown, 1993).

Linear mass shakers provide deterministic or random excitation signals in either lateral or vertical directions. However, they are expensive and cumbersome for field testing. Eccentric mass shakers only provide harmonic signals and most are designed for lateral excitation. This

device is also expensive and cumbersome for field testing. Since each of the machines mentioned must hit the surface of the bridge, traffic cannot cross while this testing is being done. Many times this results in road closures which can burden certain towns and cities depending on the traffic count of that area.

The first impact test of a steel stringer bridge was performed by Madwesh and Aktan (Madhwesh & Aktan, 1992). This provided a basis for when Aktan used the Westbound Cross County Bridge to perform vertical impact tests and horizontal forced vibration tests. The goal of this study was to determine the critical response mechanisms of the bridge such as natural frequencies, damping, mode shapes, deflections, strains and rotations. Some of these calculations were even measured at abutments, piers and along the girder. Analytical and measured frequencies were compared by using a priori model and a calibrated model, respectively, as well as the experimental results. Even though a unique analytical model could not be created, it was still important to "complete" the three-dimensional model with all of the correct boundary, continuity and existing conditions, along with geometry, so that the 3-D displacement kinematics could be simulated. To do this, additional static loading of four trucks (50 kips each) were used in various configurations along the bridge. This study found that impact testing (and deriving modal flexibility) is a reliable method to determine the properties of a bridge. However, the authors observed non-linearity at service levels of a concrete slab due to deterioration; impacts should not automatically be accepted. The writers also concluded that when completing a three-dimensional, model three items need to be taken into account: 1.) limit states should govern 2.) critical elements, regions, and capacities should be established and 3.) trucks arranged in positions to maximize needs in critical regions (Aktan, 1993).

Miller performed a non-destructive test followed by a destructive test to determine the condition of the bridge and in what manner it will fail. The non-destructive test consisted of truck loading (with three dump trucks) and modal analysis using the impact hammer method. For truck loading, deflections were recorded and those corresponding to undamaged areas matched the results from the finite element model. However, the shoulders, which were damaged, did not match. Surprisingly, the results were only off by 20%, given that the top rebar was exposed. Results from the impact hammer showed that the shoulders were more flexible. This was done by striking the hammer at various grid points and developing the flexibility matrix. After doing the destructive test by loading the bridge to a maximum of 720,000 pounds, the authors found that failure was not shown by the predictive model. The failure was in a shear, but brittle manner and was of major concern to the authors. It was concluded that replacement was less cost effective and proper understanding of deterioration, failure and management would lead to more cost effectiveness (Miller, 1992).

In order to achieve a modal flexibility matrix that is structurally significant, the fundamental requirements of modal analysis must be satisfied. These include linearity, time invariance and observability. On a steel stringer bridge in Cincinnati, the system was determined to be linear by verifying that the Frequency Response Functions (FRFs) obeyed Maxwell-Betti's principle of reciprocity. The bridge materials, steel, concrete and asphalt all have stiffness's that are dependent upon temperature. Often times, conventional impact testing is time consuming and takes the majority of the day. Getting more accurate averages in less time would possibly allow for better results. Furthermore, temperature variation can lead to less accurate FRFs and ultimately less accurate modal flexibility. To ensure time invariance, it is best to test during a time period of constant temperature. After verifying that the Cincinnati bridge was time

invariant and linear, a set of quality control checks were set up in order to make sure that the data was not corrupted. With conventional impact devices, in order to generate enough energy to excite the modes of the structure, the mass of the hammer, tip stiffness and drop height (for a drop hammer) must all be at the optimal condition. Even when checking these parameters, it can still be difficult to generate a repeatable force (Lenett et al., 1997).

The monitoring of global weakening of bridge structures is used to measure the amount of damage caused by aging, deterioration, misuse, or lack of proper maintenance. This is referred to as the Global Flexibility Index and is the spectral norm of the modal flexibility matrix obtained in association with selected reference points that may be sensitive to deformation of the bridge structure. Ambient and forced vibration testing are used to help determine if deterioration is present. However, for bridge testing, ambient testing is not as substantially sufficient as forced vibration testing. It has been found that deterioration reduces stiffness and thus flexibility increases. By establishing a flexibility matrix, with respect to chosen degrees of freedom, it is possible to gain insight about deterioration (Patjawit & Kanok-Nukulchai, 2005).

Since most civil engineering structures have relatively low natural frequencies and are large in size, it makes most input-output testing challenging to achieve. Most believe that this is why improving an output only modal identification technique is needed. Other methods that may be used under operational conditions include using finite element correlation analysis, defining a dynamic baseline for the undamaged structure, integrating output only practices into health monitoring, and applying vibration control devices (Cunha & Caetano, 2006).

"Rapid" Multi-Reference impact testing was performed by Lenett et al. in Ohio on a two lane, steel stringer bridge. This type of multiple reference impact test had to be done so that traffic

was not halted. To obtain accurate results, impacts must be done with no traffic on the bridge so that noise is minimized. Each lane was tested at six locations. The test itself took approximately one hour. The reliability of flexibility derived from this form of testing was compared to simulated and actual truck loading displacements. Good correspondence was observed and the method was determined to be reliable (Lenett et al. 2002).

In New Jersey, two bridges built in the 1980s were tested via MRIT by a rebound controlled drop hammer. This device is provided in order to create large, robust impacts that create a high signal to noise ratio; overcoming noise from traffic effects. To avoid closing the bridges, a Global Structural Assessment (GSA) system is needed. This system would be used to complete a series of SIMO tests, as it travels along the bridge. The series of SIMO tests can then be integrated together to attain more complete flexibility information. It was hypothesized that the system could output between 13 and 26 tons of force. Due to time/cost requirements, a truck load test was not done. However, SISO, MIMO and global cases were considered in addition to SIMO to provide a basis for comparison. In the absence of the truck load test a finite element model was created for validation. The rebound hammer was successful in performing a MIMO test within the range of 100 Hz at 75 kN. There is still much work to be done to create an automated system for this type of testing (Liao, 2012).

Using tactile transducers, averages can be taken quicker and roads will not have to be closed because the impact will not be taking place on the surface of the bridge. Previously described devices are cumbersome, expensive, and questionable.

1.4 OBJECTIVE AND SCOPE

The objective of the proposed research is to determine whether the use of tactile transducers (also known as shakers) can be used to adequately perform Multi-Reference Impact Testing (MRIT). The main purpose of the investigation is to 1.) Determine if the transducers can produce a repeatable force so that a load cell is not needed 2.) Verify that this method's results are just as comparable to using an impact hammer, if not better. Theoretically, tactile transducers (TT) will be able to produce the same input force repeatedly. With an impact hammer, it is quite difficult to generate the same force several times because it is dependent upon human effort. This inconsistency can lead to over ranging accelerometers or failing to excite the structure sufficiently.

In addition to the three main objectives described above, the author will be looking at how long the test of a full scale bridge will take. This will be compared to normal impact testing and also ambient vibration testing. Typically, impact testing requires a bridge that is free of vehicular traffic because impact locations are on the top side of the bridge. By using tactile transducers, they can be mounted to the bridge underside. This allows testing to be performed below the bridge without disturbing traffic.

CHAPTER TWO

TACTILE TRANSDUCER DYNAMIC IMPACT VALIDATION

2.1 INTRODUCTION

Recently, Dr. Kirk Grimmelsman developed a novel dynamic testing method at the University of Arkansas that utilizes tactile transducers to provide controlled dynamic excitation to civil structures. Tactile transducers (TT) are small, low-cost and lightweight devices that are more commonly used for home audio, gaming and personal entertainment purposes.   The specific tactile transducers selected for the dynamic testing system are essentially small-scale, proof mass shakers that are capable of producing both random and deterministic dynamic excitation signals. The dynamic testing system has been characterized and evaluated in the laboratory and field by a number of graduate students from Dr. Grimmelsman's research group for dynamic testing of bridges using different multiple input, random and harmonic excitation schemes (Fernstrom et al. 2013; Carreiro et al. 2013; Fernstrom and Grimmelsman 2014; and Grimmelsman et al. 2014). A primary objective of this thesis research was to evaluate the dynamic testing system as a potential alternative for multiple-reference impact testing. Impact dynamic testing of bridges and other civil infrastructure is normally performed using a broadband impulse excitation force generated by instrumented hammers or drop weights. Because the tactile transducers used for the dynamic excitation system had only been characterized and evaluated for random and harmonic excitation signals, the devices needed to be evaluated for impulsive signals before proceeding with the laboratory and field testing programs. The operational performance and capabilities of the tactile transducers were evaluated for different impulsive signal characteristics. The dynamic force generated by the devices and the optimal approach for measuring this force were also investigated. Finally, the complete setup and operation (from

signal generation to data acquisition) of the dynamic excitation system was validated prior to its use for impact testing.

2.2 PRIOR TESTING AND EVALUATION

As mentioned previously, although the tactile transducers had not been specifically used for multiple-reference impact testing purposes, others from the research group had performed laboratory studies to evaluate the operational and performance characteristics of these devices for random and harmonic excitation signals. The capabilities of these devices needed to be systematically evaluated under controlled conditions since they are not specifically intended for experimental modal testing applications. The force output, stroke length, armature mass, effective frequency range, etc. were unknown for these devices. Various tactile transducers were evaluated in the laboratory to determine their operating and performance characteristics and these were compared to the performance of a conventional linear mass shaker (APS 113HF). Fernstrom et al. (2013) and Carreiro et al. (2013) describe the laboratory evaluation studies conducted for the tactile transducers and the results. These studies indicated that the APS shaker produced a larger force in general, but most effectively between 4 Hz and 50 Hz. The tactile transducer force increased linearly between 1 and 29 Hz from 0 to 20 lbf, respectively. Due to a short stroke length, the force that can be produced is limited up to 25 Hz. Furthermore, the force is also limited by the capacity of power at higher frequencies.

Carreiro et al. (2013) checked the uniformity of twelve tactile transducers by comparing the time and frequency domain characteristics. This was done by creating a random input signal in MATLAB where 60,000 random numbers were selected from the normal distribution with an RMS value of unity. After transforming to the frequency domain, a fifth order Butterworth filter was applied with a cutoff frequency of 50 Hz. Additionally, a low pass filter at 20 Hz was

applied because below this frequency the tactile transducer is limited by stroke movement. The resulting signal was sent to each tactile transducer three times and the force output was recorded by load cells. Phase characteristics were consistent but amplitudes had more variation. In the frequency domain, mean force and variance were computed at each frequency line. The variance was off by about 7% of the mean force across the spectrum of frequencies. All tactile transducers proved to perform similarly but not identically. Even though only one tactile transducer is to be used for the research herein, future studies may require deployment of a full array of devices.

Signal reproduction characteristics were also assessed by generating Gaussian white noise in MATLAB, sending it through a power amplifier, and then to a tactile transducer. Both the measured output signal and measured shaker force output were transformed to the frequency domain. The resulting normalized power of the measured input signal was shown to be higher than that of the tactile transducer which means that there was some filtering of random noise. Excitation at lower frequencies is limited due to the short stroke length of the tactile transducer. However, full response is essentially provided by 10 Hz. The tactile transducer produces maximum power at its own natural frequencies. Therefore, as the input frequency becomes greater than the natural frequency, the power falls off. This proves that by using a pure sinusoidal signal, the response of the device to random signals can be predicted. Uniformity will not be perfect throughout the input range and the signal is affected by the shaker itself (Carreiro et al., 2013).

The evaluations discussed above were based on sinusoidal (harmonic) and Gaussian white noise signals. Multiple reference impact testing utilizes broadband impulsive excitation and thus the findings from these prior studies are not strictly applicable to the present study.

However, the impulsive excitation signals necessary for multiple-reference impact testing have different time and frequency domain characteristics. Nonetheless, the properties of the tactile transducer found by other researchers will be considered and kept in mind as a basis devices.

2.3 SIGNAL SELECTION

2.3.1 Square Wave Generation

Two different signal types were considered to decide which would be best for impact testing using the tactile transducers. A square wave signal was initially thought to be the best choice for doing continuous impacts with a set amount of time between each one. When using a square wave, there was only one load cell used and it was held between two wooden plates by a metal rod. Considering, time domain data, one could see that each hit alternated in magnitude. For instance, the first impact may be 95 lbs. of force and the next 90 lbs. It was also hard to predict whether the tactile transducer would impact in the upward or downward direction first. To determine the consistency, 20 low and 20 high impacts were taken. This same approach was attempted using three load cells in a tripod configuration, but the results were similar.

2.3.2 Impulse Generation

After determining that a square wave created more work than necessary, an impulse signal was considered. There were five different methods considered when generating the impulse signal. For each of these methods, the signal was created in MATLAB as a text file, imported into Signal Express as an analog signal, generated via the Peripheral Component Interconnect (PCI) eXtensions for Instrumentation (PXI) system. The generated signal was looped from the analog output directly into the analog input channel of the PXI system. Each various text file was formed in MATLAB by creating a matrix with a specific impulse value in the first row followed by zeroes. This is referred to as the measured input signal and was a length of 1000. Time- and

frequency-domain characteristics were examined. Theoretically, the signal measured by the PXI should have the same amplitude as the signal created in MATLAB because it is what Signal Express is generating. This same measured signal should be transmitted to the tactile transducer using Signal Express, the PXI, and the amplifier. The load cells will measure the force that the tactile transducer outputs.

Case 1 consisted of using a unit impulse that is generated at 1000 Hz as an analog signal via the PXI, and also measured by the PXI at 1000 Hz. For Case 2, a unit impulse of 1000 Hz was created and then a Low Pass Filter (LPF) was applied at 100 Hz. This case was considered because the PXI cannot directly generate a signal less than 1000 Hz. For this research study, the frequency band of interest is DC to 100 Hz, so a signal of only 200 Hz is needed. Case 3 was similar to Case 2 because it dealt with generating the signal at 1000 Hz, but only using frequency content of 100 Hz. However, instead of applying a LPF, the Subset and Resample command in Signal Express signal was utilized. Case 4 was the same as Case 1, except that two unit impulses were created. Case 5 was the same as Case 2 except, there were two unit impulses filtered.

2.3.3 Device and Signal Selection

After reviewing the time and frequency domain characteristics of the measured signal and also the force measured by the load cells it was determined that using the National Instruments PXI DAQ platform did not yield desirable results. By investigating the different signal cases described above, it was observed that generating the impulse signal at 1000 Hz did not produce a large enough impact needed to excite a full-scale bridge. Several factors were manipulated when attempting to produce an appropriate impact level. For instance, in Signal Express the "Gain" step can be used as a multiplier of the amplitude. However, whether changing the amplitude manually or via the "Gain" step in Signal Express, the output cannot be above 10 V; this

property cannot be changed. While using a generation rate of 1000 Hz, the experimenter was unable to produce an effective impact. With that said, the only other option was to reduce the generation rate and use a 16-bit analog output device. By switching to this device to complete the study, impulses of values higher than one were used.

2.4 FORCE PLATE CONFIGURATION

While completing the signal generation study a few different setups were considered. This dealt with the plate material that would be used to hold the load cells in place and also attach the tactile transducer. The first design consisted of two wooden plates attached by a stainless steel rod and a single load cell. This design proved to be too loose and unstable and did not produce adequate results. Next, two wooden plates separated by three load cells in a triangular configuration were studied. This design was adequate, but the input force was not equally distributed among the three force transducers. Balancing the force transducers so that each read close to the same force became the next goal. This goal was also of importance because if the force could be equally distributed, it would eliminate the need for three force transducers per force plate. It would be assumed that each transducer reads a third of the total load. Additionally, more tactile transducers could be used and would reduce setup time. Furthermore, the third configuration became a wooden bottom plate and a stainless steel plate that attached to the bottom of the tactile transducer as shown in Figure 2.1. Unfortunately, the load cells could not be balanced so that each load cell received an equal portion of the total load. Consequently, the final load cell/tactile transducer set up consisted of two wooden plates, six studs, and three load cells shown below in Figure 2.2.

Figure 2.1. Force transducers between stainless steel and wooden plates (Photo by author)

Figure 2.2. Final tactile transducer setup (Photo by K. Grimmelsman)

CHAPTER THREE

LABORATORY TESTING PROGRAM

3.1 INTRODUCTION

Prior to testing a full-scale, in-service structure, it is necessary to understand how testing is carried out. Laboratory testing gives an idea of results that may be acquired in the field. The main goal is to determine the modal parameters of the structure using an impact and a tactile transducer, then compare the results. It also allows preparation for potential problems that may arise during field testing. For this research Multiple Reference Impact Testing (MRIT) of a large steel structure (grid) in a controlled laboratory environment was completed. This was done using a small impact hammer and a tactile transducer

3.2 GRID MODEL STRUCTURE

The grid model simulates a simply supported bridge and allows researchers to perform several different types of tests. It consists of three longitudinal girder lines made of W8x10 steel sections. There are seven transverse lines also made of W8x10 steel sections. The total length is 27 ft. and the width is 9 ft. as shown in Figure 3.1.
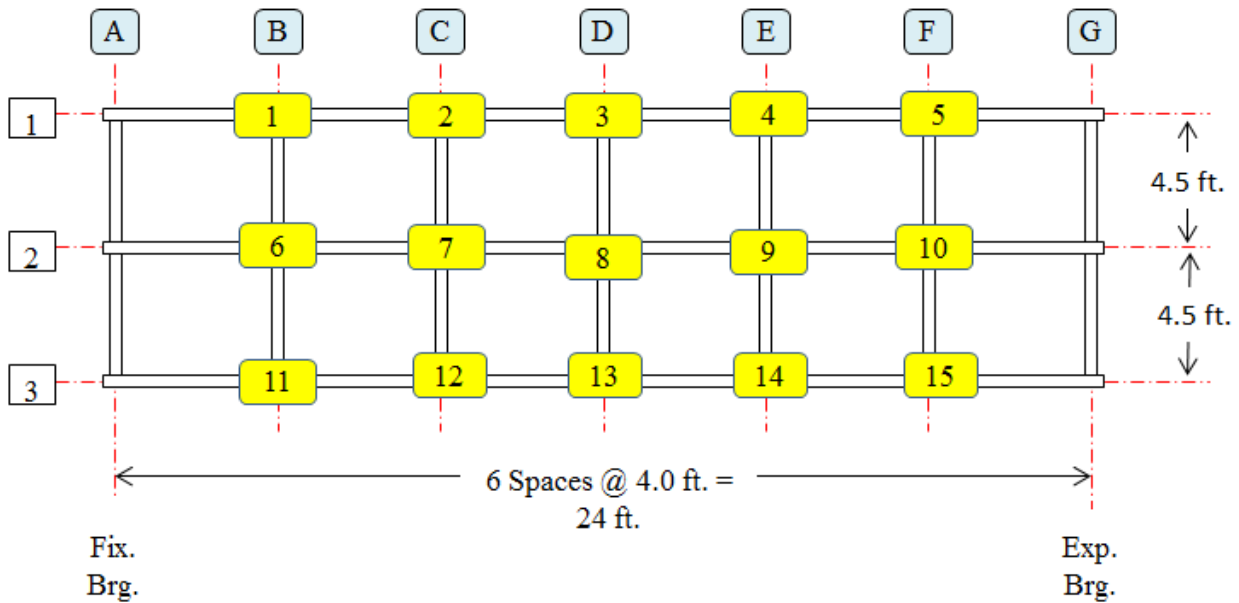
Figure 3.1. Grid model layout

3.3 EXPERIMENTAL PROGRAM

3.3.1 Input/Output of Grid

For this laboratory test, there were 15 input locations and 15 output locations (Degrees of Freedom). Each input location was excited one at a time for both the hammer and the tactile transducer (shaker) test. Moreover, at each input location, there was a PCB Piezotronics 393C accelerometer used. The specific location and properties of each accelerometer can be seen in Table 3.1. Accelerometers were attached to the underside of the grid via a magnet.

20

Table 3.1. Grid accelerometer properties

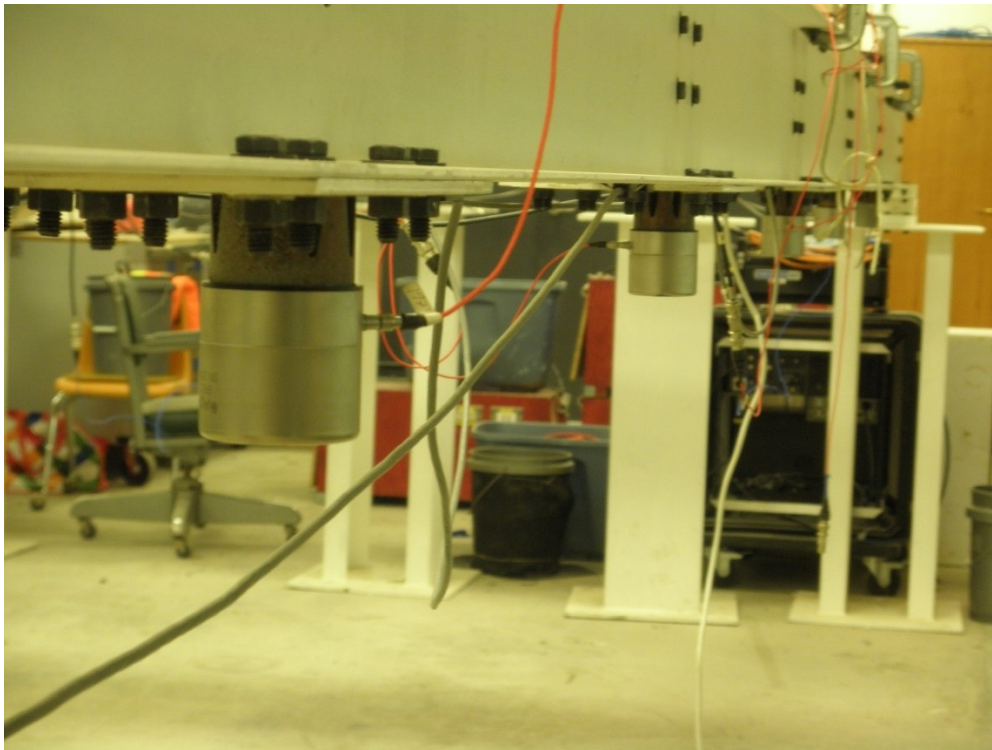| Grid Location	Serial Number	Type	Sensitivity	Range (g's)
1	8957	393C	1050.34	± 2.5
2	23271	393C	1054	± 2.5
3	23606	393C	1057	± 2.5
4	23721	393C	1044	± 2.5
5	23607	393C	1042	± 2.5
6	23753	393C	1067	± 2.5
7	23608	393C	1061	± 2.5
8	23526	393C	1070	± 2.5
9	23444	393C	997	± 2.5
10	23523	393C	1089	± 2.5
11	23501	393C	1110	± 2.5
12	23500	393C	1097	± 2.5
13	8204	393C	1066.39	± 2.5
14	23502	393C	1081	± 2.5
15	23522	393C	1070	± 2.5

Figure 3.2. Accelerometers attached to underside of grid (Photo by author)

3.3.2 Input Device Descriptions

To perform the laboratory hammer test a small PCB Piezotronics hammer was used to excite the structure. The model number is 086C03. The hammer comes with four different tips of varying hardness; stainless steel being the hardest, white being medium, red as soft and black super soft. Typically, a hard tip will provide the sharpest peak and the best looking frequency spectrum after transforming to the frequency domain. However, the stainless steel and white tips were not used because the accelerometers were easily over-ranged. Furthermore, the red tip provided the most suitable impact and was used to complete the test. The tip is installed directly onto the 0.6 in. hammer head, in front of the load cell. At the end opposite of the load cell, an extender cap was installed to provide more weight. The hammer load cell has a peak input range of ± 500 lbf and a sensitivity of 10.76 mV/lb.
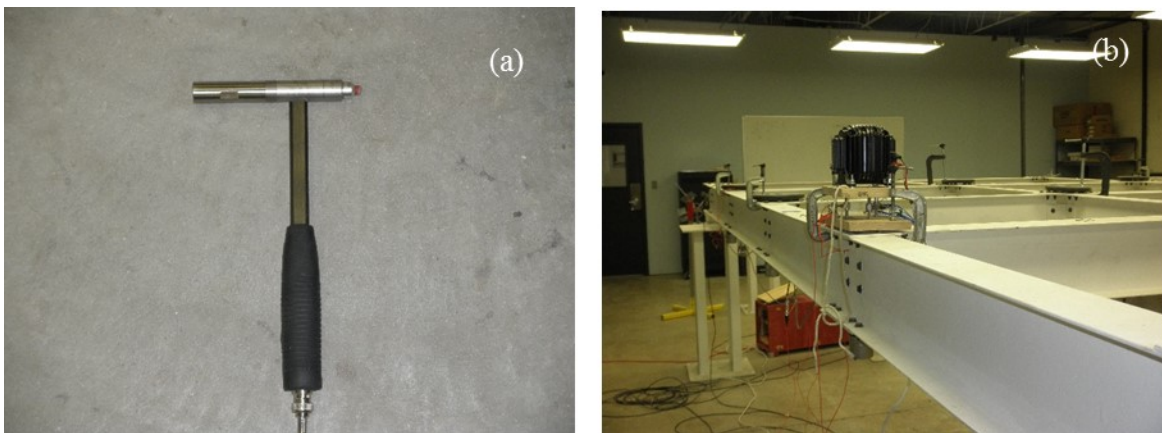
Figure 3.3. (a) Small impact hammer and (b) tactile transducer (Photo by author)

The tactile transducer configuration uses three force transducers which are all model number 208C02. The input range for all three force transducers is ±100 lbf and the sensitivities for the force transducers used are 48.27 mV/lbf., 47.91 mV/lbf., and 45.74 mV/lbf. Each load cell is 0.625 in. x 0.625 in. x 0.5 in. size and 0.80 oz. and made of stainless steel.

3.3.3 Data Acquisition System

While completing the hammer impact test on the grid structure, the only data acquisition equipment needed was the hammer, accelerometers and National Instruments DAQ 9234 (NI 9234). The NI 9234 contains 24 channels with minimum and maximum sampling rates of 1.652 kHz and 51.1 kHz, respectively. For this particular test a total of 16 channels was required; fifteen channels were used for the accelerometers and one channel for the impact hammer. LabVIEW Signal Express was used to record the input force and output accelerations. The sampling rate was 1.652 kHz.

During the shaker test, a total of 18 channels were needed because of the three load cells being used along with the shaker. A 10 V analog signal was created using Signal Express and then converted to a digital signal by a 16 bit analog output device. After being converted, the signal was transmitted to an amplifier and then ultimately sent to the shaker which excited the structure. This input excitation was recorded by the three force transducers and the resulting accelerations were recorded by the accelerometers.

3.3.4 Conduct of Testing

To ensure comparable results when executing the laboratory study, it was essential to simulate the weight of the tactile transducer at every output location. By adding ten pound weights at each point on the grid, the researchers were able to accomplish this. When performing the hammer test, there were weights at all 15 output locations whereas with the shaker, all locations except the driving point contained the ten pound weight. A good impact is defined as one that did not over-range any of the accelerometers nor the load cell of the hammer or tactile transducer. At each driving point, the researcher collected fifteen and twenty good impacts using the hammer and a shaker, respectively. All of the impacts were recorded via Signal Express and

converted to a text file. To ensure, good frequency resolution and adequately spaced data sets, approximately twelve seconds were recorded between each impact. When using the hammer, a stopwatch was used to tell the researcher when to make another impact on the structure. As a result, the hammer impacts are not all exactly twelve seconds apart. Contrarily, the shaker impacts are exactly at twelve seconds due to it being executed by Signal Express. Good resolution was also sought by manually ranging the output response. For instance, at a driving point the response range is expected to be higher because the device is impacting that point. However, at other points on the structure, the range is less because the excitation is taking place further away.

After gathering all fifteen or twenty good impacts at every input location, the text files were separated to get only one impact in every file and separate the good impacts from the bad ones. This was done by extracting 0.5 seconds before the impact peak and then 11.5 seconds after.

CHAPTER FOUR

FIELD TESTING PROGRAM

4.1 INTRODUCTION

The purpose of completing this field test is to determine the modal parameters of a full-scale, in-service bridge. It is necessary to complete this test in addition to the laboratory test because the structure is more massive and the responses are more unpredictable. The results that are received will be compared to tests that were completed in the past. Since this bridge is subject to climate changes and temperature effects, natural frequencies, damping ratios, mode shapes and modal flexibility can give insight as to whether the bridge is changing over time. MRIT testing was completed using a large sledge hammer and a tactile transducer.

4.2 TEST STRUCTURE

Hancil "Tiny" Hartbarger Memorial Bridge was the structure selected for this MRIT study. It is located in Fayetteville, AR on Black Oak Rd and was built in the 1980s. Hartbarger Bridge consists of ten simply supported spans and carries two lanes of traffic (one in each direction) over the West Fork of the White River. Each span is 50 ft. long totaling to 500 ft. The width is approximately 27 ft. The reinforced concrete deck is supported by W27x94 rolled steel beams. There are four longitudinal beams and five transverse beams. This bridge is ideal for testing because it resembles a similar structure as most of the bridges in the United States. Hence, successfully testing this bridge in a new manner means that it could be applied to many of the others around the country.

Figure 4.1. (a) Road view and (b) underside of bridge (Photo by author)

4.3 EXPERIMENTAL PROGRAM

4.3.1 Input/Output of Structure

Previous field tests used the second span for testing. However, due to excess water that collected over a series of rain events, the third span had to be utilized. For this field test, there were 20 input and 20 output locations. All sensor locations were in between nodal points as seen in Figure 4.2. This was done to capture all possible modes. Similar to the laboratory study, all accelerometers used were PCB Piezotronics 393C. The accelerometers were attached to the top flange of the beams in the same fashion as the grid study. Accelerometer locations and properties can be seen in Table 4.1.
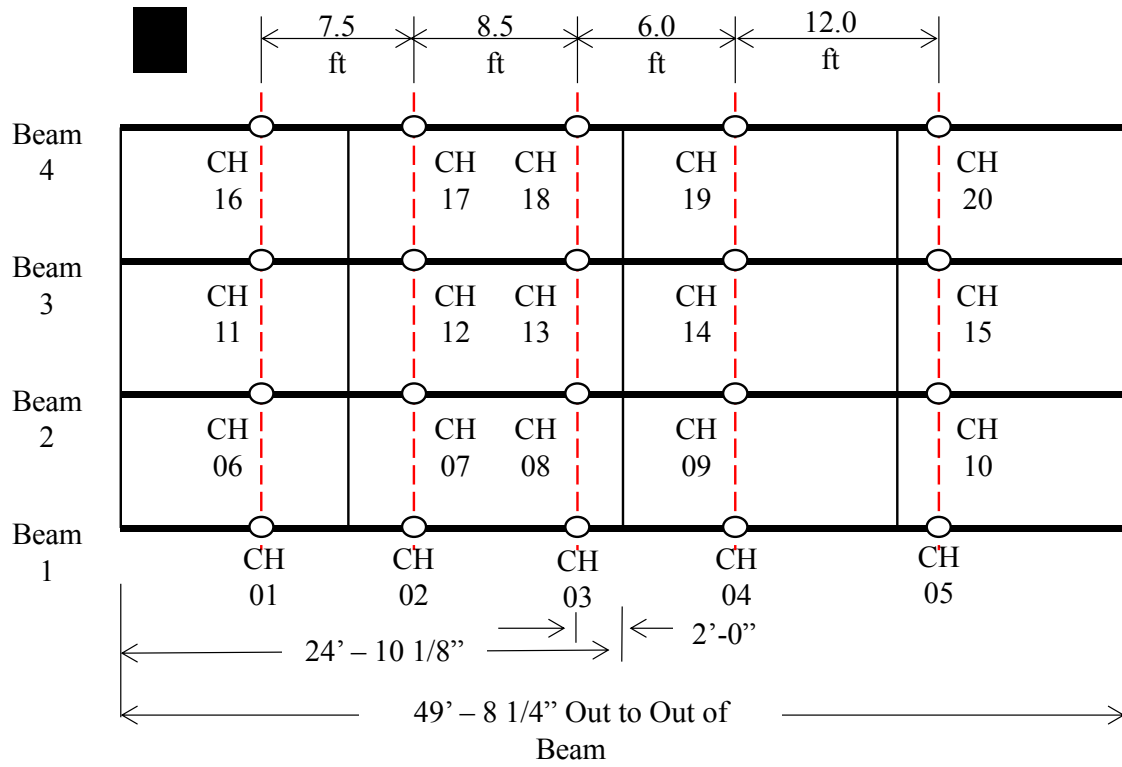
Figure 4.2. Span 3 sensor locations

Table 4.1. Hartbarger accelerometer properties

Bridge	Serial	Type	Sensitivity	Range (g's)
1	23501	393C	1110	± 2.5
2	23500	393C	1097	± 2.5
3	8204	393C	1066.39	± 2.5
4	23502	393C	1081	± 2.5
5	23522	393C	1070	± 2.5
6	23753	393C	1067	± 2.5
7	23608	393C	1061	± 2.5
8	23526	393C	1070	± 2.5
9	23444	393C	997	± 2.5
10	23523	393C	1089	± 2.5
11	8957	393C	1050.34	± 2.5
12	23271	393C	1054	± 2.5
13	23606	393C	1057	± 2.5
14	23721	393C	1044	± 2.5
15	23607	393C	1042	± 2.5
16	23499	393C	1071	± 2.5
17	23752	393C	1073	± 2.5
18	23525	393C	1081	± 2.5
19	23443	393C	1096	± 2.5
20	23717	393C	1031	± 2.5

4.3.2 Input Device Descriptions

The hammer portion of the field test was completed with a sledge hammer that is a PCB

Piezotronics model number 086D50. The hammer comes with four tips that each have a certain

hardness. The red tip, which is considered soft, was used to complete the test. The sensitivity is

1 mV/lbf and the input range is ±5000 lbf. The 3 in. diameter head weighs twelve pounds and

the length of the hammer is 35 in. The tactile transducer used in the field was the same as the

one used in the laboratory study. Figure 4.3 shows the sledge hammer and exactly how the

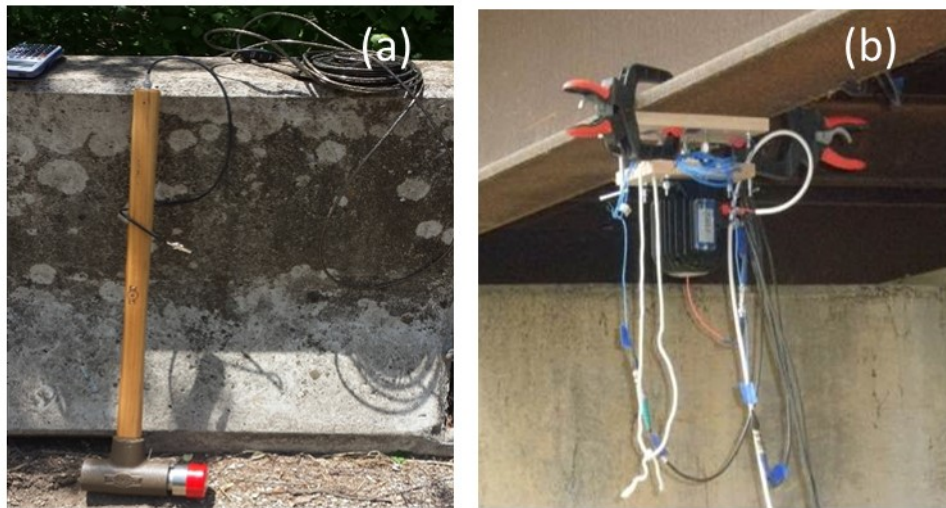shaker was clamped to the underside of the bridge at each input location.

Figure 4.3. (a) Sledge hammer and (b) tactile transducer (Photo by author)

4.3.3 Data Acquisition System

Similar to the grid hammer test the only data acquisition equipment needed was the hammer, accelerometers, and NI 9234. Except now, 21 of the 24 channels were used; with channels 1-20 being used for accelerometers and channel 21 for the sledge hammer. LabVIEW Signal Express was also used during the field test to record the excitation force created by the sledge hammer and output responses acquired by accelerometers. The sampling rate was 1.652 kHz.

During the shaker test, 23 channels of the NI 9234 system were used. Besides the use of more channels during the field study, the data acquisition system was exactly the same as the grid shaker test.

4.3.4 Conduct of Testing

The process for conducting both the hammer and shaker test in the field are similar in that each input location is excited one at a time. However, since Hartbarger was not closed to perform the test, there was a need to take note of traffic effects.

4.3.4.1 Hammer

Unlike the grid hammer test, the field hammer test required the researcher to make impacts on the top side of the concrete deck. Prior to performing the investigation, measurements were taken to determine where accelerometers were located in relation to the bottom of the concrete parapet. Each sensor location was marked with chalk and denoted by its respective location number. In general, impact testing cannot be done while traffic is crossing because the data is corrupted with noise. For safety purposes, when traffic was crossing the bridge, impacts were not imparted. As a result this made identifying and separating impact files quicker and easier; this will be discussed at the end of this section. Despite no traffic, when impacts were taken, the researcher still had to keep track of "good" and "bad" impacts. A good impact is defined as one with no traffic, no over-ranged accelerometers or over-ranged force transducers. If not careful, it is quite easy to over-range accelerometers even on a full scale bridge. For the duration of the test, each impact was marked as either good or bad. The goal for the hammer test was to get at least 10 good hits at each input location. When traffic was not crossing the bridge, a stopwatch was set for eight seconds to alert the researcher when to perform another impact.

4.3.4.2 Tactile Transducer

Opposite of the field hammer test, the shaker test was done under the bridge. With that said, testing at a specific location was never halted due to traffic. However, alertness was critical when marking impacts as good or bad. A camera was installed at the top of the bridge to record

and allow the researcher to determine when traffic was approaching. It was still necessary to take note of how soon or how late traffic crossed the bridge in relation to when the shaker impacted the structure. The shaker was programmed to impact the bridge every eight seconds. The goal for the shaker test was to get at least 20 good hits. After 20 good hits were attained, the shaker was taken down and moved to the next impact location.

After getting the desired 15 or 20 good impacts at all 20 locations, the recorded text files were separated into individual data sets with 0.5 seconds before the peak impact and 6 seconds after the peak.

CHAPTER FIVE

RESULTS AND DISCUSSION

5.1 DATA ANALYSIS PROCEDURE

Data analysis of the studies described in the previous chapters took place in three major steps: 1.) assembling the frequency response functions (FRFs) from the measured input-output data; 2.) identifying natural frequencies, damping ratios, modal vectors, and modal scaling; 3.) determining modal flexibility from identified modal properties. Beginning with pre-processing of raw, time domain data, MATLAB was used for all data processing.

5.1.1 Compilation of the Frequency Response Function

As stated in the previous chapter, after collecting data from all input points it was necessary to extract the "good" data. This part of the data analysis is referred to as pre-processing. Even though each impact was separated by a certain amount of time, the full time record may not have been needed; if the adjacent impact was corrupted with noise from traffic, extracting too many samples after the desired peak may cause noise to be extracted as well. However, before considering the amount of time or samples, the preferred frequency resolution had to be decided. Frequency resolution is defined by the spacing between frequency lines when using the Fast Fourier Transform (FFT) to determine characteristics in the frequency domain. Frequency resolution is determined by:

$$\Delta f = \frac{1}{N * \Delta t}$$

Equation 5.1.

Where:
Δf= the frequency resolution in Hz
N= the block size (or length) of the data set (also known as the NFFT)
$\Delta t = \frac{1}{Fs}$, Fs is the sampling frequency, in Hz

Having a good frequency resolution helps eliminate leakage and quantization errors (Allemang, 1999). The block size of the data should be its respective length before transforming to the frequency domain using the FFT command. The researcher wanted a frequency resolution as close to or less than 0.1 Hz as possible. Block sizes used in the frequency domain should always be powers of two. For instance 4,096; 8,192; 16,384; and 32,768 are all powers of two used as the block size before transforming to the frequency domain. Often times, extracted data in the time domain may fall in between two of the block sizes mentioned. When this is the case, it is necessary to "zero pad" the data in order to reach the next closest block size. For hammer and shaker laboratory tests, the data was 19,825 samples or approximately 12 seconds long and the sampling frequency was 1,652 Hz. In order to make the data 32,768 samples long, the initial data had 12,943 zeroes added to it.

After using the FFT to transform to the frequency domain, the H_1 algorithm was used to compile the FRFs (He & Fu, 2011). The H_1 algorithm is computed by doing:

$$H1 = \frac{GXF}{GFF}$$ Equation 5.2.

Where:

$GXF = X(\omega) * conj(F(\omega))$

$$GFF = F(\omega) * conj.(F(\omega))$$

5.1.2 Complex Mode Indicator Function

To derive modal characteristics, the Complex Mode Indicator Function (CMIF) was used to identify possible modes of the structure by "peak picking." CMIF utilizes Singular Value Decomposition (SVD) of the compiled FRFs. The selected peaks are natural frequencies plotted from singular values in the CMIF plot. The algorithm used to compute the singular values is:

$$[H(\omega)] = [U(\omega)][\Sigma(\omega)][V(\omega)]'$$ Equation 5.3.

Where:

$[H(\omega)]$ =frequency response function

$[U(\omega)]$ = left singular vector matrix

$[\Sigma(\omega)]$ = singular value diagonal matrix

$[V(\omega)]$ = right singular vector matrix

The strength of the response at each mode is directly proportional to the singular values. Each singular value that is picked has a corresponding left singular vector that is the shape of the estimated mode. Furthermore, to get the singular values, SVD is only performed on the imaginary portion of the FRFs (Fernstrom et al., 2013).

5.1.3 Enhanced Frequency Response Function

After completion of SVD, the left singular vectors associated with the peak singular values are used as filters to abridge the measured responses to the amount of single-degree-of-freedom (SDOF) systems that were chosen as singular values. This is a transformation from physical space to modal space. Enhanced frequency response functions (eFRFs) are then expressed for each SDOF to enhance the contribution of the respective mode while suppressing the effects of other modes. Normally, to calculate the eFRF for a particular mode, s, the FRF is premultiplied by the transpose of the left singular vector, $\{U\}^T$, and postmultiplied by the modified right singular vector, $\{V_{mod}\}$. However, using the right singular vector will corrupt modal flexibility, will taint unit mass normalized vectors and will not preserve right scaling. To eliminate this issue the pseudoinverse of $\{V\}$ and driving points of $\{U\}$ are multiplied to create a modal scaling factor. Therefore,

$$\text{msf}= \{V\}^+_{1xNi} * \{U(at\ driving\ pts.)\}_{Nix1} \qquad \text{Equation 5.4.}$$

and

$$\{V_{scaled}\} = msf * \{V\}. \qquad \text{Equation 5.5.}$$

Once the modal filters are used to make the physical to modal space transformation, the process

in Equation 5.6 is used to uncouple the system into a vector of SDOF modes, s.

$$\{eH(\omega_i)\}_s = \{U\}_s^T$$
$$* \left[[\Psi] * \left[\frac{1}{j\omega_i - \lambda_r} \right] * [L]^T \right] * \{V_{scaled}\}_s \right]$$

Equation 5.6.

Where:
$\{eH(\omega_i)\}_s$ = enhanced frequency response function
$$j=\sqrt{-1}$$
λ_r =rth complex eigenvalue or system pole, $\lambda_r = \sigma_r + j\omega_r$
$[\Psi]$ = modal vector

The product of $\{U\}$ and the modal vectors $\{\Psi\}$ determines the extent of enhancement. A sharp

peak is depicted in the eFRF if the two vectors are completely uncoupled. This is the result of

the two vectors being mutually orthogonal. However, if they are not orthogonal, other modes

will have contribution and appear in the plot as well.

5.1.4 Modal Parameter Computation

The natural frequencies chosen from the CMIF plot are simply estimates. Using each SDOF

system, the modal frequency, damping, and scaling can be obtained and are treated as scalar

values. Using Equation 5.7, a least squares method can be applied to solve for the poles of the

SDOF system. The variable a_2 or a_0 must be assumed to be equal to 1. The eFRFs and $j\omega^n$

quantities are known.

$$[(j\omega_i)^2 * a_2 + (j\omega_i) * a_1 + a_0]\{eH(\omega_i)\}=[(j\omega_i)^2 *$$
$$b_2 + (j\omega_i) * b_1 + b_0]\{R(\omega_i)\}$$

Equation 5.7.

Where:
$R(\omega_i)$ = index vector
a_i = components of the coefficient matrix [A]
b_i = components of the coefficient matrix [B]

5.1.5 Modal Scaling

Now that the poles have been solved for via a mode-by-mode basis, modal scaling can be formulated using Equation 5.11. The left singular vector and mode shape vector are close approximations of each other. A relationship is defined via Equation 5.8 through Equation 5.10.

$$\{U\}^T_{1 \, x \, No} * \{\Psi\}_{No \, x \, 1} = s_{1k} \qquad \text{Equation 5.8.}$$

$$\{U\}^T_{1 \, x \, No} * \{\Psi\}_{No \, x \, 1} = s_{1k} \qquad \text{Equation 5.9.}$$

$$Q_r * \{\Psi_{drv.pt}\}^H_{1xNi} * \{V_{scaled}\} = Q_r * s_{2k} \qquad \text{Equation 5.10.}$$

Where,
Q_r = scaling term associated with mode k
s_1 and s_2 are scalar values for mode k.
The scaling formulation becomes

$$eH(\omega_i) = \frac{s_{1k} * Q_k * s_{2k}}{j\omega_i - \lambda_k} \qquad \text{Equation 5.11.}$$

The term Q_r is solved using the least squares method (Catbas et al., 2004).

5.1.6 Modal Flexibility

The final step, modal flexibility, can be completed using a system of algebraic equations. The process begins with taking the Laplace Transform of the equation of motion shown in Equation 5.12 and assuming zero initial conditions.

$$[M]\{\ddot{x}(t)\} + [C]\{\dot{x}(t)\} + [K]\{x(t)\} = \{F(t)\} \qquad \text{Equation 5.12.}$$

Where:
[M] = system mass matrix
[C] = damping matrix
[K] = stiffness matrix

[F(t)]=external force vector

$\{\ddot{x}(t)\}, \{\dot{x}(t)\}, \{x(t)\}$ = accelereation, velocity, and displacement vectors respectively

The inputs of the system divided by the outputs represents the transfer function of the system in

the Laplace domain. The FRF [H(ω)] is now represented as [H(s)]. The formulation is shown in

Equation 5.13.

$$[H(s)] = \frac{\{X(s)\}}{\{F(s)\}} = \frac{1}{s^2 + [M] + s[C] + [K]}$$

Equation 5.13.

X(s) = displacement in the Laplace domain
F(s) = force in Laplace domain

When assessed along every frequency line, the FRF can be obtained again and takes the form

$$[H(\omega)] = \frac{1}{-\omega^2[M]+j\omega[C]+[K]};$$

Equation 5.14.

Notice that s=jω. If evaluated at ω=0, the flexibility matrix [K]$^{-1}$ is found. The FRF can be

further synthesized from the modal parameters shown in Equation 5.15. This solves the

flexibility matrix for the system (Fernstrom et al. 2013).

$$[H(\omega)] = \sum_{r=1}^{N} \frac{\{\Psi\}_r * \{\Psi\}_r^T}{M_{Ar}(j\omega - \lambda_r)} + \frac{\{\Psi\}'_r * \{\Psi\}_r'^T}{M_{Ar}(j\omega - \lambda'_r)}$$

Equation 5.15.

5.2 LABORATORY RESULTS

5.2.1 Time Domain Comparison

For comparative analysis, it is important to know how the impact hammer and tactile transducer

(shaker) behave before beginning to extract the modal parameters. This will give insight as to

why there are certain characteristics in the frequency domain. As stated in previous chapters, a

typical impact of a hammer in the time domain should consist of one sharp peak as shown in

Figure 5.1a. The bottom half of the figure shows the response of the 15 output locations. As

expected the largest blue spike represents the sensor that was located at the driving point (impact

location). The response using the tactile transducer is similar to that of the hammer, however the input force appears quite different. When inspecting the time domain of the tactile transducer, it can be seen (Figure 5.2a) that there is motion for about 100 samples before the actual impact occurs. This is caused by initial movement of the shaker. After the impact, there is still some movement from the tactile transducer. Unlike the hammer, after the impact, the shaker is still attached to the structure which causes additional free vibration to appear in the figure.

5.2.2 Frequency Domain Comparison

When considering the input during impact testing, a broad flat spectrum is desired after transforming each impact to the frequency domain. The frequency resolution corresponding to the laboratory study was 0.0504 Hz. Figure 5.3a shows a typical FFT of an impact on the grid structure. Figure 5.3b is a typical response spectrum where the peaks represent the frequencies that were excited during this specific impact at this location. Figure 5.4 is the result of taking the FFT of impact data on the grid using the tactile transducer. The spectrum is not as smooth and flat as that of the hammer due to the pre-impact movement (seen in the time domain) and also the free vibration type response due to the structure and shaker itself. However, when comparing the two devices, the magnitude of the shaker response at some frequencies is higher than that of the hammer. This means that at input location ten, the shaker was able to excite the structure more than the hammer. When examining other input locations throughout the structure, this is true as well.
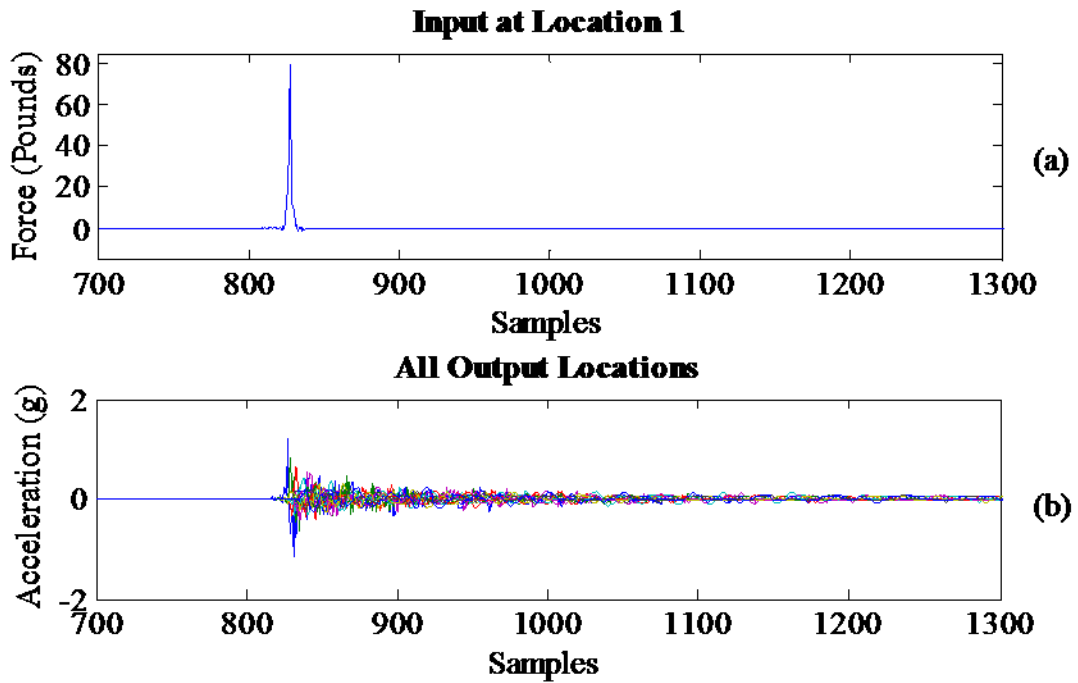
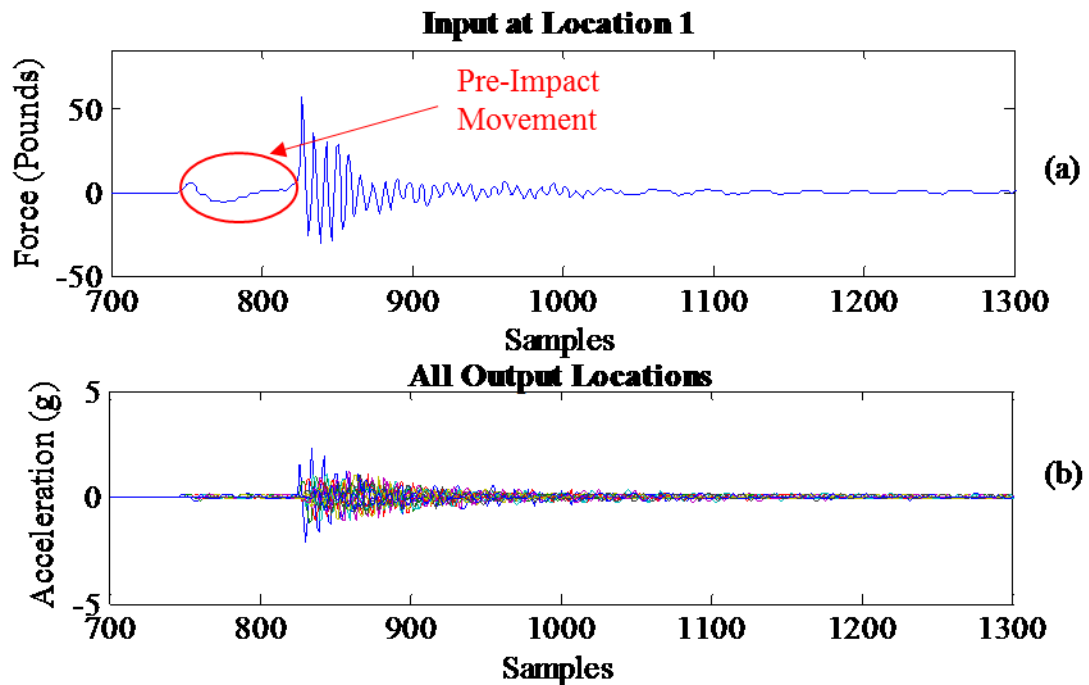**Figure 5.1. Hammer time domain (a) input force and (b) output accelerations**

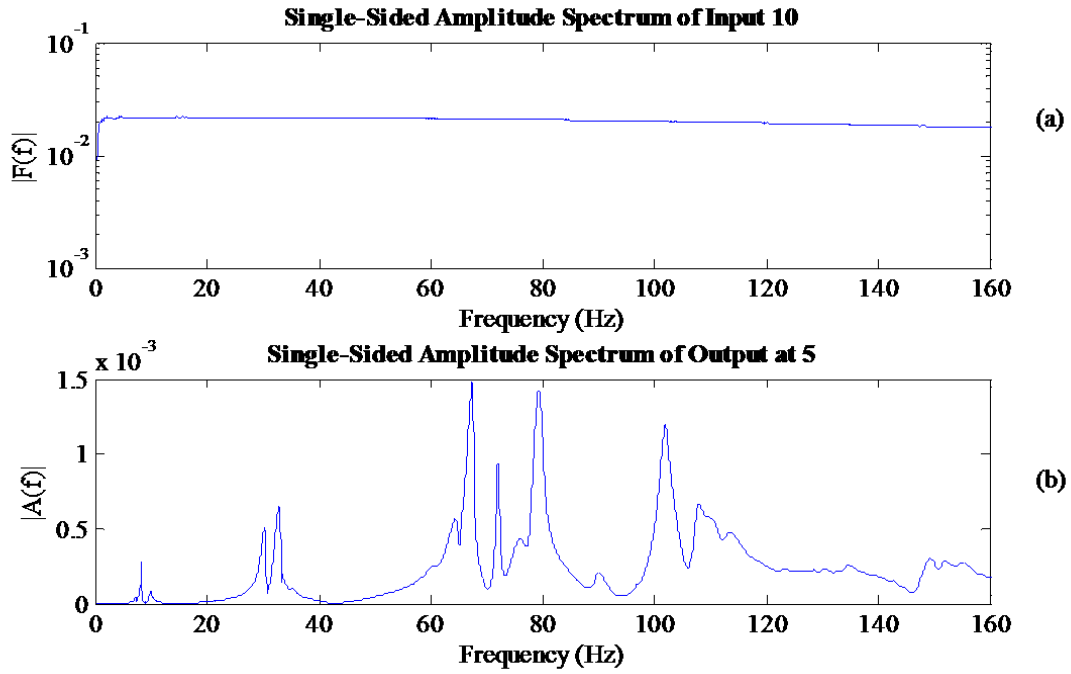**Figure 5.2. TT time domain (a) input force and (b) output accelerations**

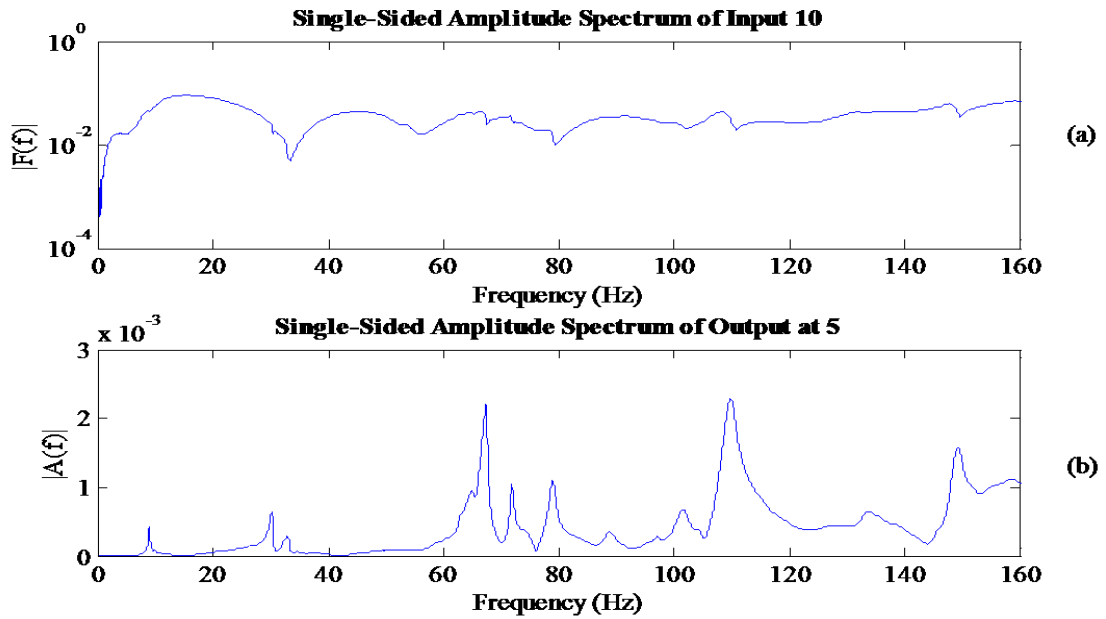**Figure 5.3. Hammer frequency domain (a) input force and (b) output acceleration**

Figure 5.4. TT frequency domain (a) input force and (b) output acceleration

5.2.3 Frequency Response Function and Coherence

Along with the advantages of impact testing that make it a simple technique to perform, there are other disadvantages that cause issues when it comes to data processing. For instance, it is difficult to control the input force level and also the range of frequencies. This can cause a poor signal to noise ratio (He & Fu, 2011). Due to the lack of ability to control the input level, it is common practice to take several impacts (also referred to as averages). With real data, noise exists at both the input and the output and affects the FRF measurements. To cancel these noise effects, Equation 5.2 is implemented. Even with this computation all noise cannot be eliminated.
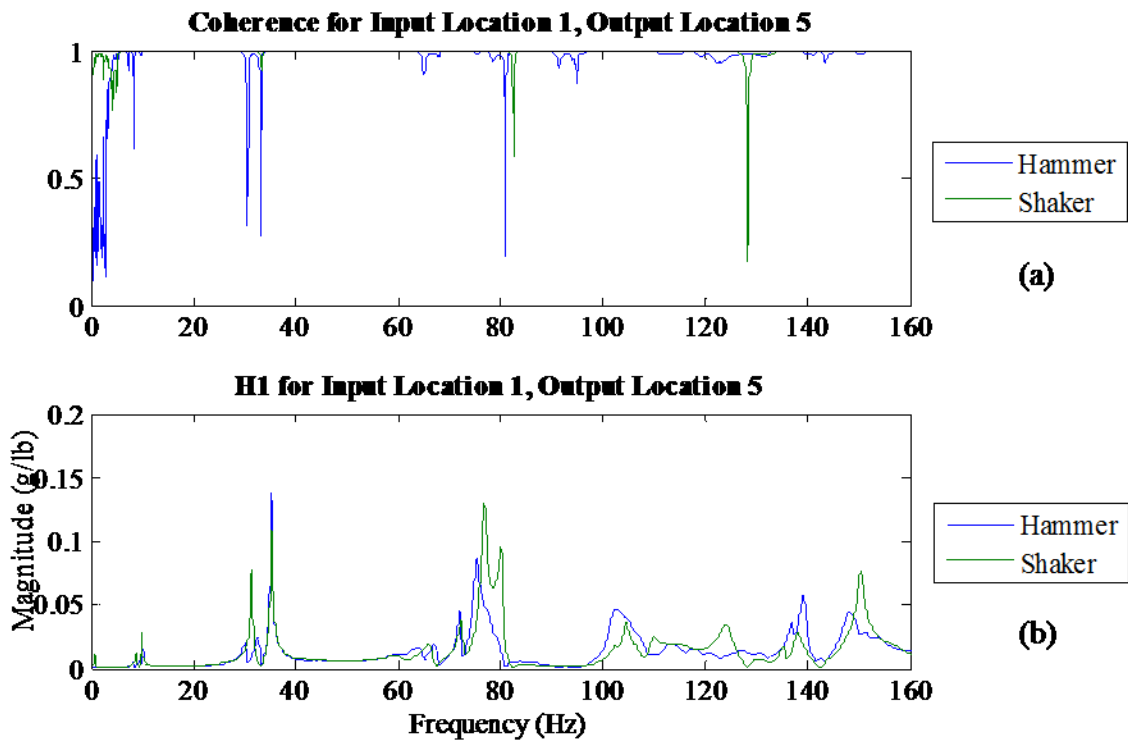

Figure 5.5. Hammer and TT comparison of (a) Coherence and (b) FRF

To determine if response is correlated to the input, coherence can be calculated using Equation 5.16 below for the *ith* output and *jth* input. This measure ranges from 0 to 1, where 1 means that the output is due solely to input and 0 means that the input does not relate at all to the output.

$$\gamma_{ij}^2 = \frac{|GXF(i,j)|^2}{GFF(j,j) * GXX(i,i)} \qquad\qquad \text{Equation 5.16.}$$

Figure 5.5 depicts a comparison of the coherence and FRF between grid data from the shaker and hammer. Both have relatively good coherence over the frequency spectrum. However, the hammer seems to display a DC component at lower frequencies. A low pass filter was used to eliminate some of this noise. The two different instruments identify frequencies close to each other in the FRF plot. For most of the FRF plot, the magnitude of the tactile transducer is greater than that of the hammer. The FRF plot gives an idea of where possible modes may be located. At these frequencies, the coherence is one or very close to it. Furthermore, not all frequencies will have a peak at every input location. For instance, impacts at midspan (locations 3, 8, and 13) may not identify, Bending 2, because at this mode these locations are nodal points. Therefore, when looking at the FRF, little to no response will be shown. To pinpoint and display all modes throughout the structure at once, the Complex Mode Indicator Function (CMIF) must be used. This will be discussed in further detail in the next section.

5.2.4 Modal Analysis Discussion

By comparing Figure 5.6 and Figure 5.7 one can tell that there is considerable noise. Typically, a CMIF plot shows that the majority of the peaks in the first singular value (top curve) and the others flatten out. This is not the case for either one of the plots.
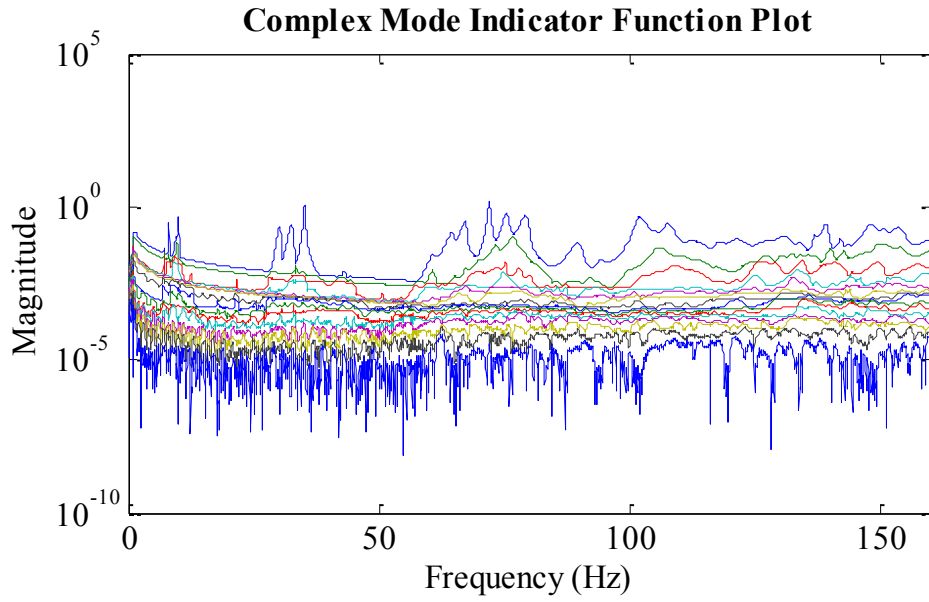
Figure 5.6. Hammer- Complex Mode Indicator Function Plot
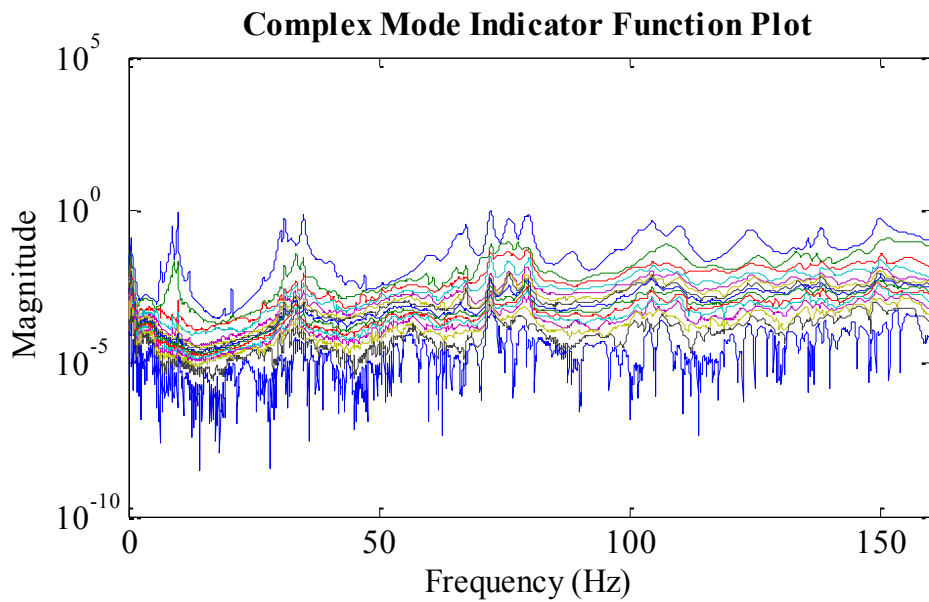
Figure 5.7. Shaker- Complex Mode Indicator Function Plot

Both plots are used to find the estimated mode shape frequencies. The physical shape of these modes are identified and plotted. They can be seen in Figure 5.8 and Figure 5.9. Along with these figures are Table 5.1 and Table 5.2 which describe the name, frequency, and damping

43

value associated with each mode. Both methods of testing were successful in finding twelve

modes.

Figure 5.8. Hammer mode shape plots

Figure 5.9. Shaker mode shape plots

Table 5.1. Identified modal parameters via impact hammer

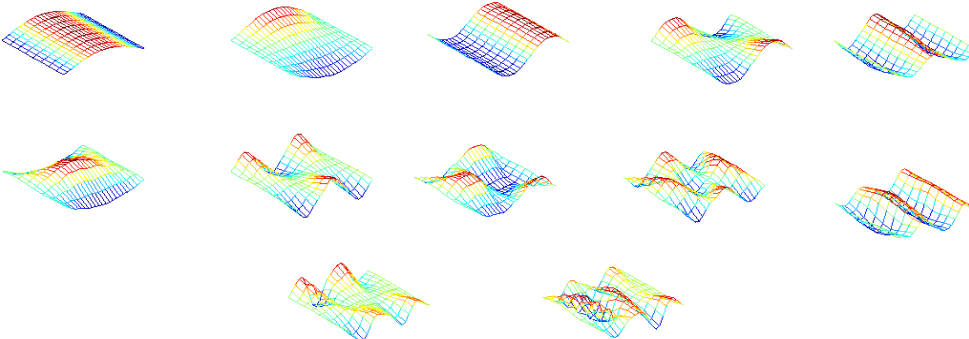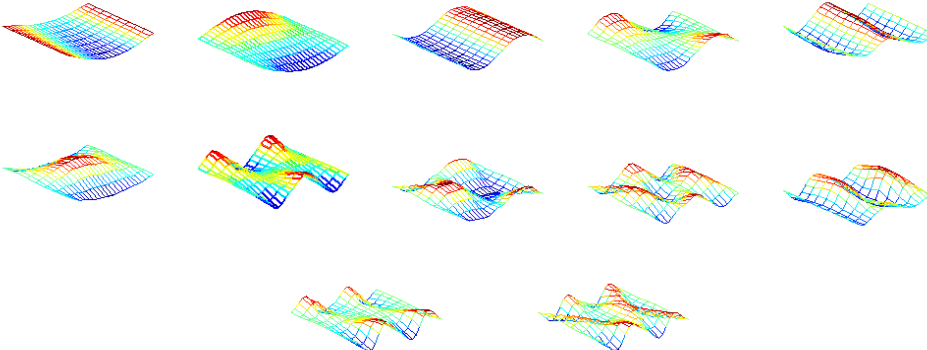| Mode	Frequency, Hz.	Damping, %	Description
1	8.12	0.712	Bending 1
2	10.03	0.975	Torsion 1
3	32.76	1.210	Bending 2
4	35.17	0.463	Torsion 2
5	67.35	0.734	Bending 3
6	72.02	0.348	Butterfly 1
7	75.46	0.810	Torsion 3
8	79.35	1.055	Butterfly 2
9	101.93	1.074	Butterfly 3
10	107.61	1.079	Bending 4
11	131.55	1.809	Torsion 4
12	153.73	1.050	Butterfly 4

Table 5.2. Identified modal parameters via TT

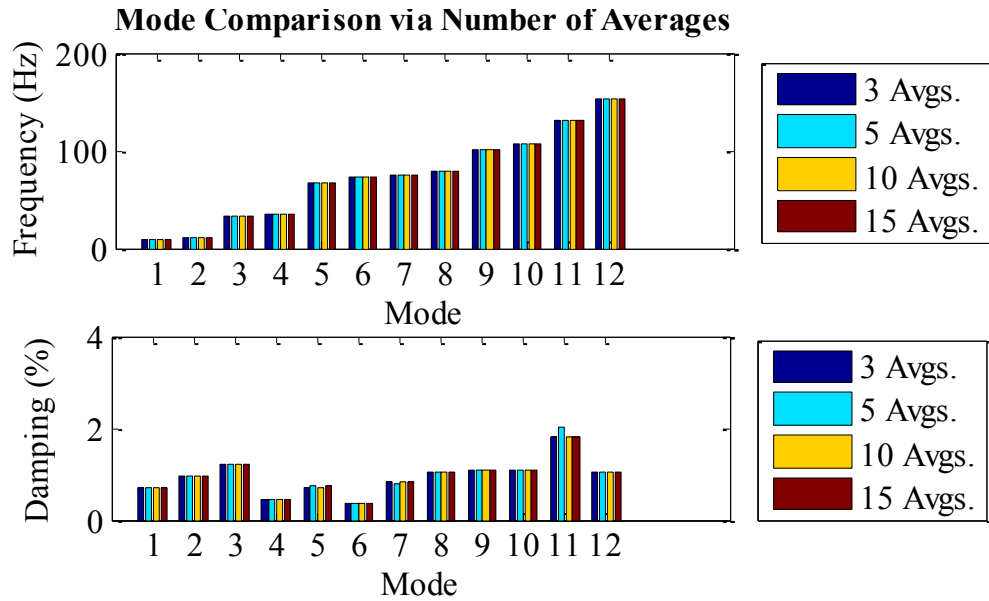| Mode	Frequency, Hz.	Damping, %	Description
1	8.86	1.233	Bending 1
2	9.87	0.543	Torsion 1
3	31.22	0.676	Bending 2
4	34.89	0.684	Torsion 2
5	67.47	0.591	Bending 3
6	72.30	0.533	Butterfly 1
7	75.95	0.977	Torsion 3
8	80.09	0.575	Butterfly 2
9	101.87	2.211	Butterfly 3
10	110.34	1.150	Butterfly 4
11	138.34	0.520	Torsion 4
12	150.14	0.733	Butterfly 4

Figure 5.10. Hammer modal comparison via number of averages

Mode shape figures shown above start with mode one in the top left corner and end with mode

twelve in the bottom right. Mentioned previously, one notable issue with impact testing is the

inability to repeatedly produce the same input force and frequency spectrum. As a result of this

issue, multiple averages are needed when processing. For the hammer laboratory study, 15 good

impacts were taken at each driving point. However, during data processing, three, five, and ten

averages were considered to see how this may affect frequency values and damping ratios. This

is represented in Figure 5.10 and Figure 5.11 . The frequencies found for each varying amount

of averages are consistent for all twelve modes. This is true for the shaker as well. Damping on

the other hand is consistent with some modes and not in others. The first four modes are able to

identify approximately the same damping ratios. After the fourth mode the damping ratios begin

to fluctuate more. Mode 11 by far has the biggest fluctuation which is shown with five averages.

The shaker average comparison is just as inconsistent as the hammer. However, the two

different methods of testing identify the modes with quite different damping ratios. For instance,

the shaker identified mode one with a damping ratio between 1.229% and 1.233% for all of the

averages. This same effect can be seen in other averages. A statistical comparison is made in

Table 5.3 and Table 5.4 to show the relationship between the number of averages used to form

the FRF. Considering the hammer statistics, the largest standard deviation is 0.1124 for Mode

11. The shaker data's largest standard deviation is 0.046 for Mode 11. When comparing Mode

11 for the hammer and shaker data, considering three, five, ten and fifteen averages when, it is

clear that these values are completely different. This leads to the assumption that there may have

been some sort of error that occurred when identifying this mode. The 95% confidence interval

range for different modes is a lot wider for the shaker. This shows that when using the shaker,

more data is needed in order to give insight about damping values. Since the hammer had a

smaller range of standard deviations and confidence intervals, it was used as a basis for

calculating percent error. It was noticed that damping values calculated for modes two, three,

five, eight, eleven, and twelve were all less than the hammer damping values. All others were

greater. Percent error for modes two, three, five, eight, eleven, and twelve range from
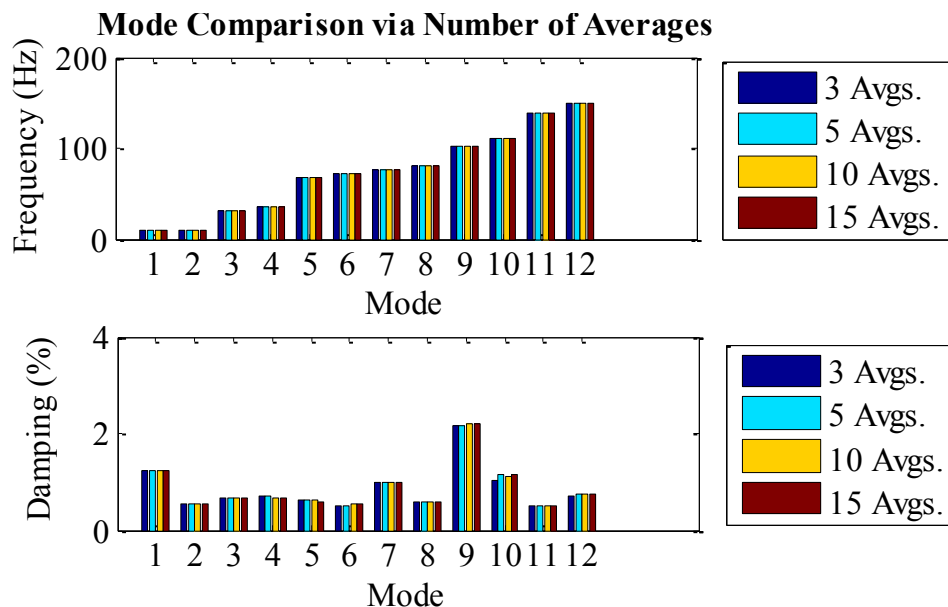
approximately 13% to 75%.

Figure 5.11. Shaker modal comparison via number of averages

Table 5.3. Descriptive statistics comparison using hammer damping values

Mode	3 Avgs.	5 Avgs.	10 Avgs.	15 Avgs.	Mean	Std. Dev.	C.I.-95%
1	0.699	0.70	0.708	0.712	0.706	0.0056	0.0089
2	0.974	0.974	0.976	0.975	0.975	0.0009	0.0014
3	1.196	1.199	1.204	1.210	1.202	0.0059	0.0094
4	0.463	0.463	0.463	0.463	0.463	0.0003	0.0004
5	0.698	0.734	0.693	0.734	0.715	0.0223	0.0355
6	0.350	0.350	0.351	0.348	0.350	0.0011	0.0018
7	0.814	0.808	0.810	0.810	0.811	0.0025	0.0040
8	1.030	1.057	1.055	1.055	1.049	0.0129	0.0205
9	1.066	1.085	1.073	1.074	1.074	0.0076	0.0121
10	1.072	1.075	1.077	1.079	1.076	0.0028	0.0044
11	1.810	2.032	1.802	1.809	1.863	0.1124	0.1789
12	1.056	1.054	1.055	1.050	1.054	0.0025	0.0040

Table 5.4. Descriptive statistics comparison using shaker damping values

Mode	3 Avgs.	5 Avgs.	10 Avgs.	15 Avgs.	Mean	Std. Dev.	C.I.-95%
1	1.229	1.23	1.232	1.233	1.231	0.0019	0.0030
2	0.544	0.543	0.543	0.543	0.543	0.0005	0.0007
3	0.670	0.674	0.676	0.676	0.674	0.0027	0.0044
4	0.690	0.691	0.684	0.684	0.687	0.0037	0.0060
5	0.634	0.633	0.614	0.591	0.618	0.0198	0.0316
6	0.509	0.525	0.529	0.533	0.524	0.0107	0.0171
7	0.981	0.980	0.977	0.977	0.979	0.0021	0.0034
8	0.573	0.573	0.576	0.575	0.574	0.0017	0.0028
9	2.156	2.173	2.209	2.211	2.187	0.0272	0.0433
10	1.046	1.134	1.121	1.150	1.113	0.0461	0.0733
11	0.512	0.511	0.509	0.520	0.513	0.0051	0.0081
12	0.724	0.729	0.733	0.733	0.730	0.0043	0.0068

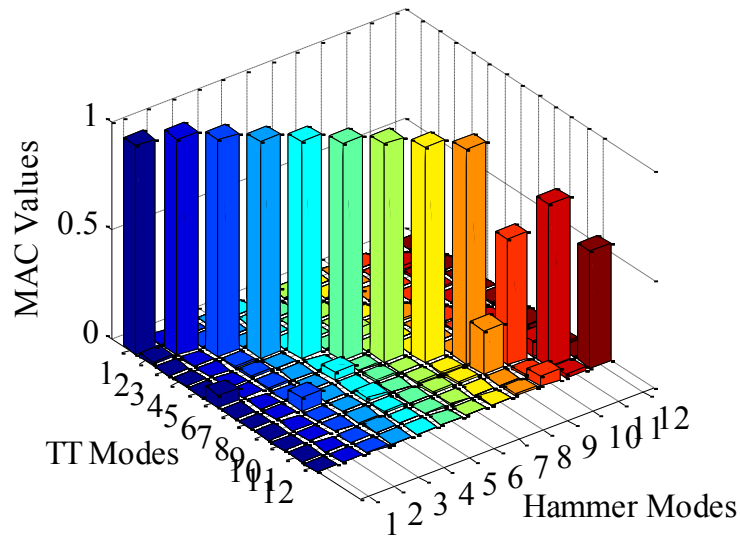**Grid Structure Modal Assurance Criterion (MAC)**

Figure 5.12. Grid structure MAC values

Modal Assurance Criterion (MAC) is a way to compare the modal vectors of two different

testing methods. For this research, MAC was computed using

$$MAC = \frac{(A' * B) * (B' * A)}{(B' * B) * (A' * A)}$$
Equation 5.17.

Where,
A= a vector of a mode shape
B= a vector of a different mode shape
'=Hermetian transpose

The left singular vectors of each respective testing method computed during singular value

decomposition are used to determine agreement between the two methods. As shown in the the

previous tables and figures, the modes for the hammer and tactile transducer are close but not the

exact same frequency meaning the vectors associated with each one is not exactly identical

(Allemang, 2003). MAC ranges from zero to one, with one meaning that there is unity and

perfect agreement between the modes of two different testing methods. Zero means the modes

do not agree at all. Considering Figure 5.12, the diagonals of a MAC plot should have values

close to one and all other terms should be nearly zero. All modes are very close to unity except

the last three which are Bending 4, Torsion 4 and Butterfly 4 and the off-diagonal terms are close to zero.

The frequency and damping values presented in Figure 5.10 and Figure 5.11 are the eFRF values computed. Figure 5.13 through Figure 5.16 show the filtered SDOFs for modes one and two for the hammer and shaker. The filtered peak is identified with a black outline and red circle in the bottom portion of each figure. The top half of each figure shows the phase angle which is the angle between the undamped natural frequency and damping ratio. When a peak is shown in the bottom plot, a change in direction of the phase angle should be noted at the same point. For the grid, Bending 1 (Mode 1) and Torsion 1 (Mode 2) are the most dominant modes of the structure. Furthermore, they are closely spaced which makes it difficult to separate even after the eFRF computation. This means that the two modes are similar in shape and that is the reason for a second, smaller peak appearing to the left of the identified one (Catbas 1997). The hammer and shaker both have well-fitting curves using the least squares method. However there is some difference between the frequency and damping values.
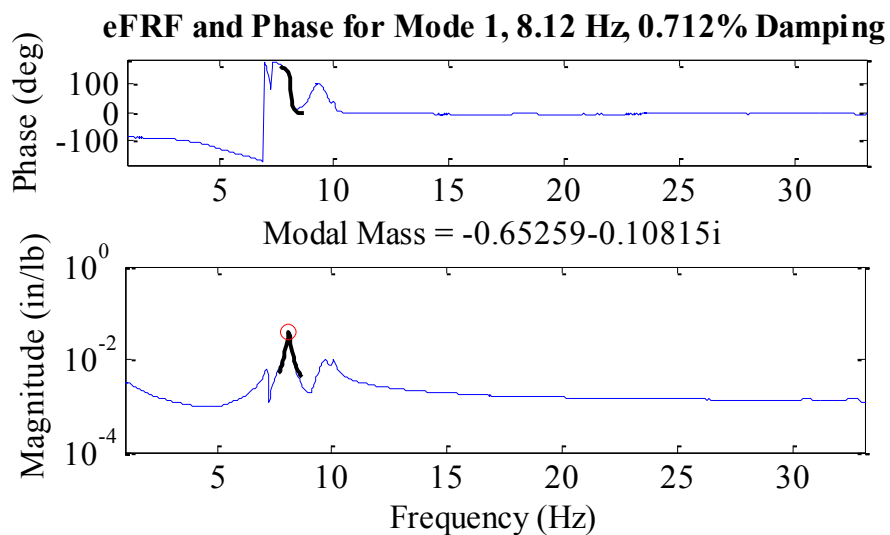

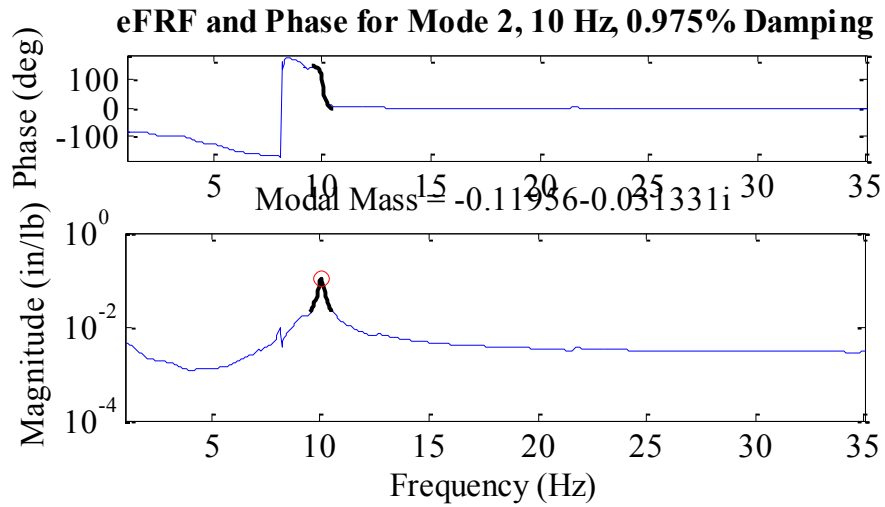Figure 5.13. Mode 1 Enhanced Frequency Response Function of hammer

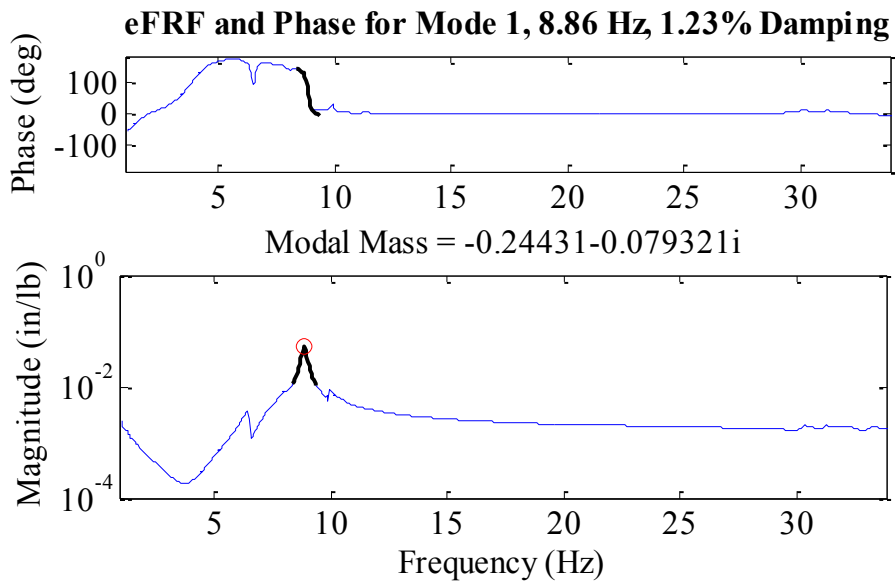**Figure 5.14. Mode 2 Enhanced Frequency Response Function of hammer**

Figure 5.15. Mode 1 Enhanced Frequency Response Function of shaker

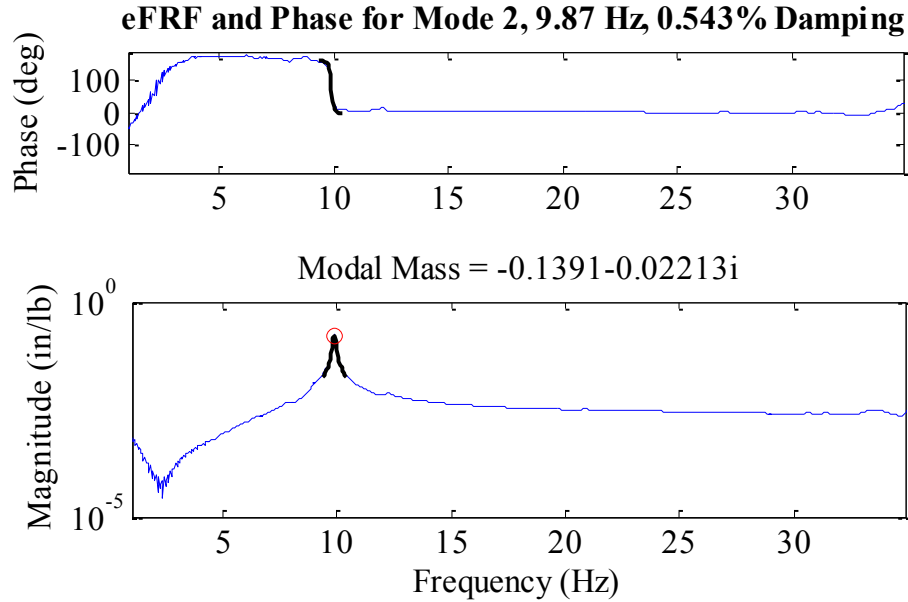**eFRF and Phase for Mode 2, 9.87 Hz, 0.543% Damping**

Figure 5.16. Mode 2 Enhanced Frequency Response Function of shaker

5.2.5 Modal Flexibility

Modal flexibility is a square matrix that is the size of the number of DOFs. In order to produce

the plots in Figure 5.17 (hammer) and Figure 5.18 (tactile transducer), a unit load was applied to

each DOF which then yielded the deflection contours shown below. Since visual inspection of

modal flexibility does not provide suitable comparison for two different testing methods, a

Frobenius norm is computed to determine the overall difference between two matrices. This

formulation is shown below.

$$D = \sqrt{\sum_{i=1}^{n}\sum_{j=1}^{n}\left(\frac{f1_{i,j} - f2_{i,j}}{f1_{i,j}}\right)^2}$$

Equation 5.18.

Equation 5.19.

$$D_d = \sqrt{\sum_{i=1}^{n}\left(\frac{f1_{i,i} - f2_{i,i}}{f1_{i,i}}\right)^2}$$

Where,
D=the value representing the overall difference between two matrices

52

D_d=the value representing the difference between the diagonals of two matrices
n=the size of the square matrices
f1=the flexibility matrix considered to be more accurate
f2=the flexibility matrix being compared

Frobenius norm calculations were completed using all terms of the matrices, D, shown in

Equation 5.18 and the main diagonals of the two flexibility matrices, D_d shown in Equation 5.19

(Fernstrom, 2014). By visual inspection the flexibility matrices represented by the two methods

are within the same numerical range but still have large values after calculating the Frobenius

norm and percent error. Diagonal comparisons yielded a pretty good value of 0.615, but the

overall matrix comparison had a high value of 1,157.39. The small D_d value and large D value

means that several of the off-diagonal DOFs do not agree by several powers of ten which is more

than likely caused by a few modes that have different modal masses and are not exactly the same
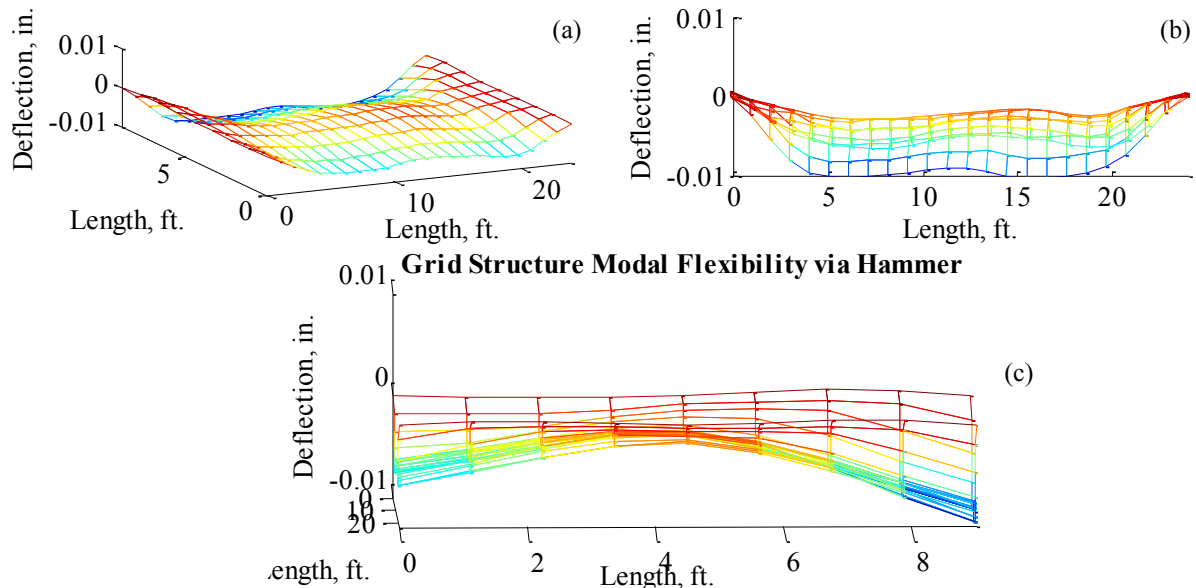
shape (Fernstrom, 2014).

Figure 5.17. Hammer modal flexibility: (a) 3D View, (b) Side View and (c) End View

53
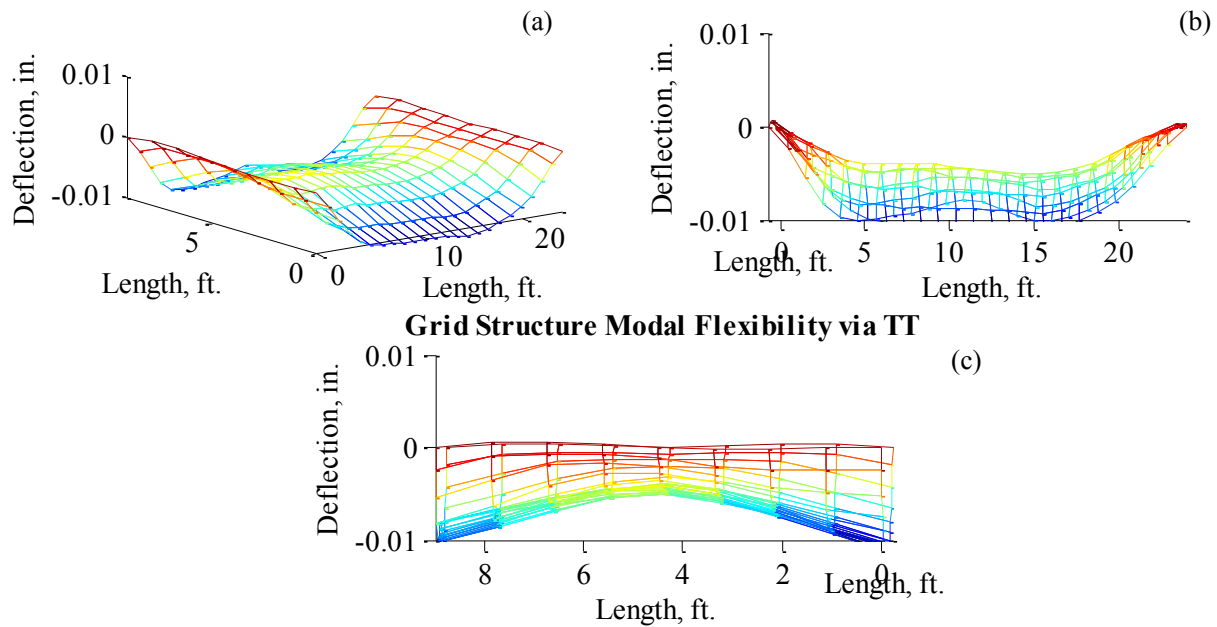
Figure 5.18. TT modal flexibility: (a) 3D View, (b) Side View, and (c) End View

5.3 FIELD TEST RESULTS

5.3.1 Time Domain Comparison

Field testing consisted of a sledge hammer test and a shaker test. The hammer test was

completed in one day and the shaker test was immediately the day after. Both days were warm

and sunny with no rain or clouds. The time domain for the hammer and tactile transducer are

shown in Figure 5.19 and Figure 5.20. The hammer time domain plot shows a sharp peak similar

to the laboratory test. The force was always over 4000 lbs. when using the sledge hammer. As

expected the tactile transducer behaved the same way as it did in the laboratory study. However,

due to noise and coherence issues (discussed later), a force window was applied to the shaker

input force. The difference can be seen in the lower portion of Figure 5.20. When applying a

54

force window, unwanted samples (noise) are multiplied by zero, and the part that is kept is multiplied by one. In this case, the largest peak is what is desired. The output responses are not affected in any manner. The free vibrations in the force signal that are seen occur because the tactile transducer is attached to the bridge even after the impact is created. Data sets with additional vibrations due to traffic are considered bad impacts and are shown in Figure 5.21. These impacts were not used in data processing. When analyzing Figure 5.21, keep in mind that the three input forces measured by the load cells have not yet been added together to get the total force. Notice that the range is from -100 to 100 compared to Figure 5.20 where the total is shown and the range is -500 to 500. The output responses below the input show the acceleration due to the tactile transducer impact first, and then the traffic disturbance. Toward the middle of the time duration, the structure experiences the largest vibrations which even cause the load cells to pick up these vibrations.

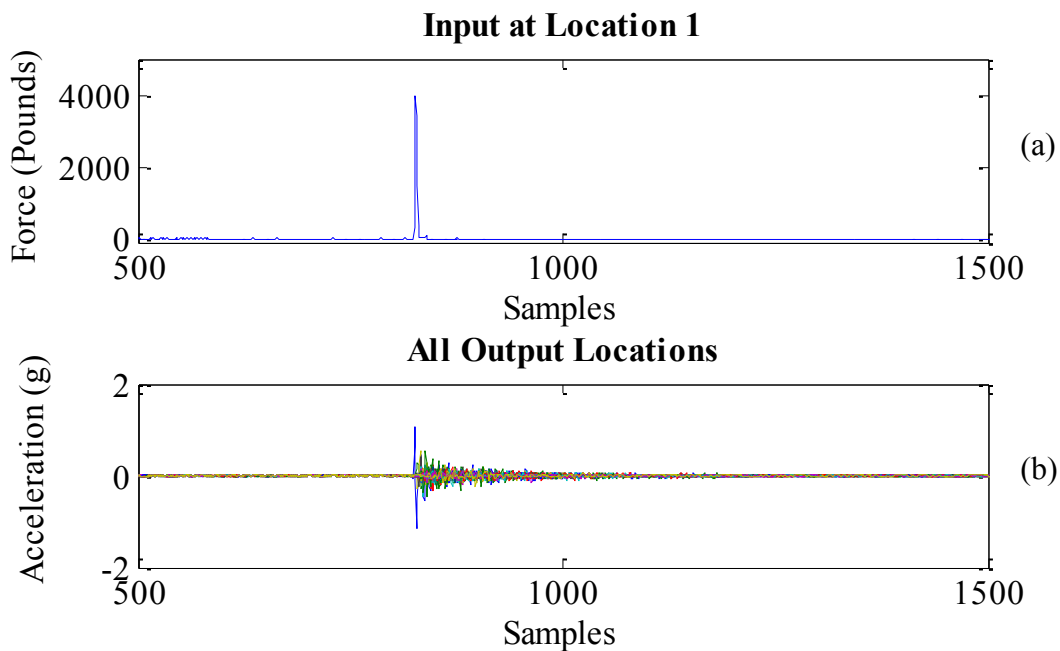**Figure 5.19. Hammer time domain (a) input force and (b) output accelerations**

55
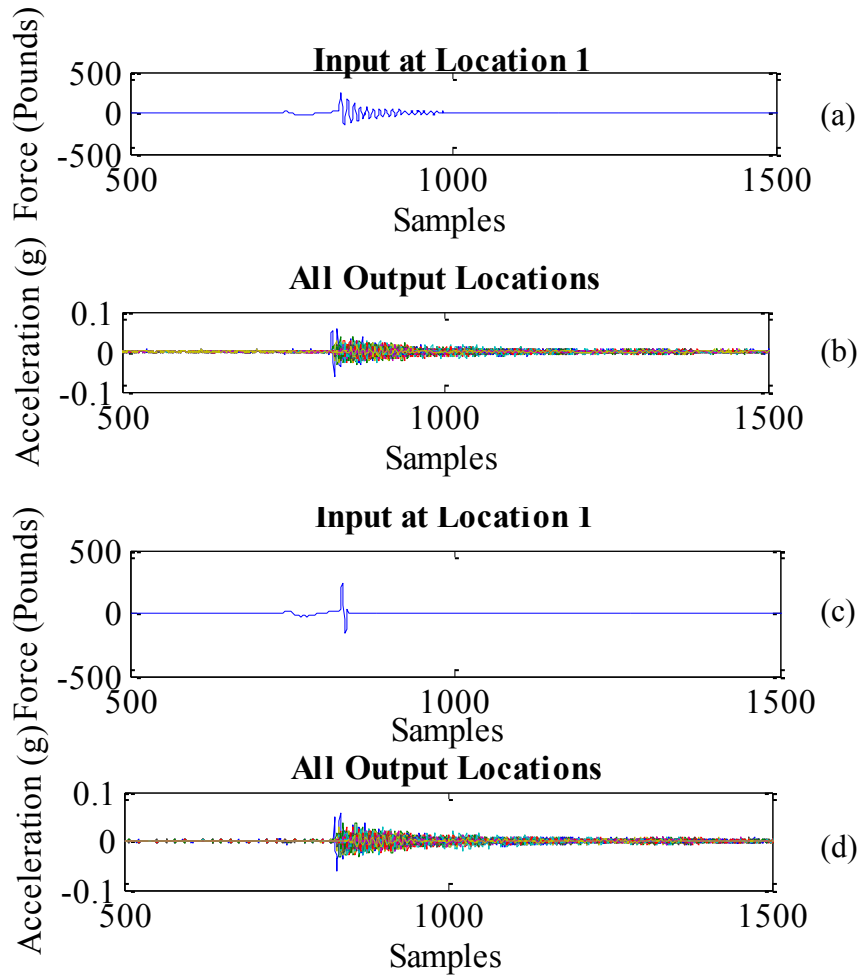
Figure 5.20. TT (a) non-windowed input force, (b) output accelerations, (c) windowed input force, (d) output accelerations
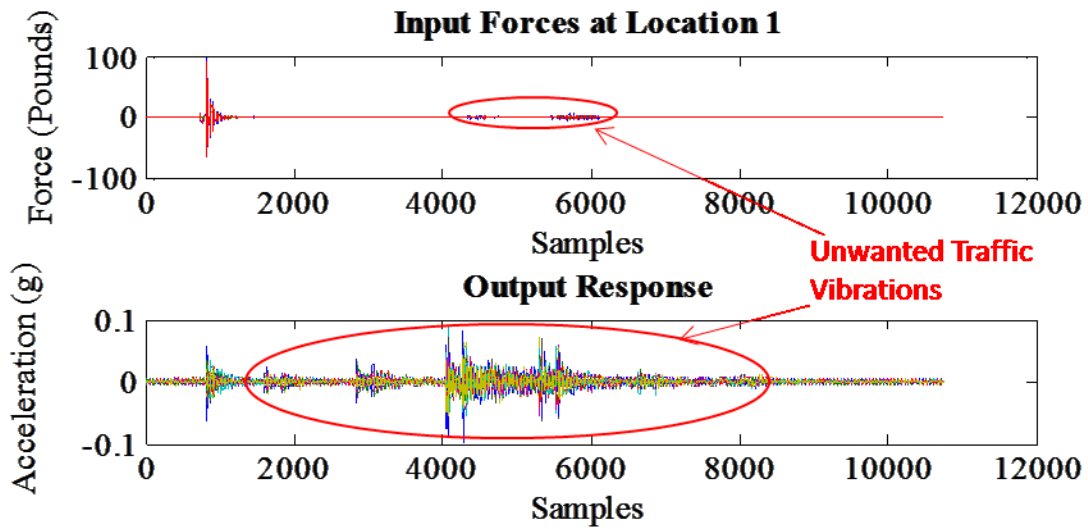
Figure 5.21. Example of a "bad" impact

5.3.2 Frequency Domain Comparison

After transforming to the frequency domain it is necessary to inspect the characteristics of each testing method to ensure that they have similarities. Considering Figure 5.22 through Figure 5.24 the frequency spectrum for the input forces look different but the responses look similar. The magnitudes of the hammer are greater than those of the shaker. This is contrary to the magnitudes of the laboratory study. However, when considering the amount of force that was used to excite the structure with each testing method, this makes sense. When performing any type of experimental or operational modal analysis, the structure is assumed to be linear, time invariant and observable (Lennett et al., 2000). The linearity of the structure means that it obeys Maxwell-Betti's principle of reciprocity. Additionally, a higher input force should result in responses with larger magnitudes.
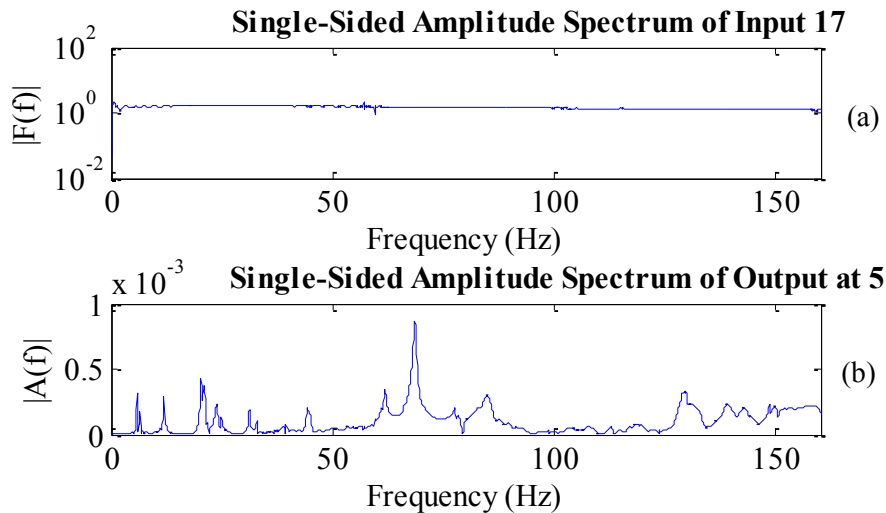
Figure 5.22. Hammer frequency domain (a) input force and (b) output acceleration
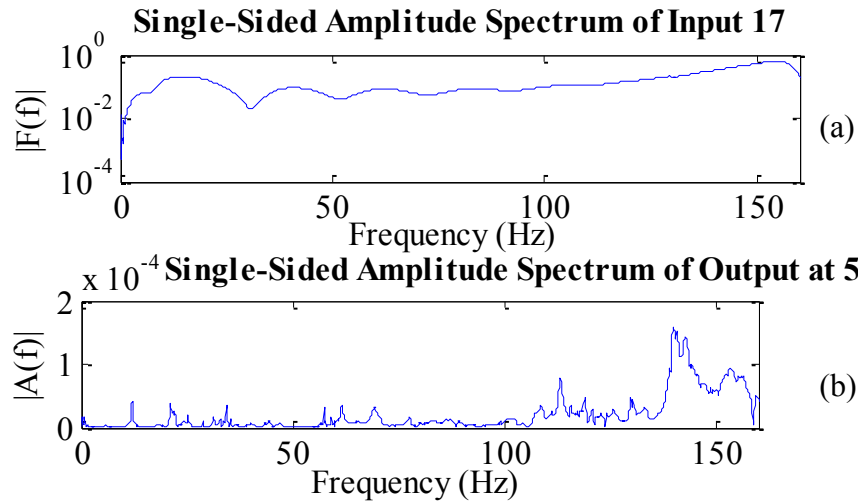
Figure 5.23. TT frequency domain (a) non-windowed input force and (b) output accelerations
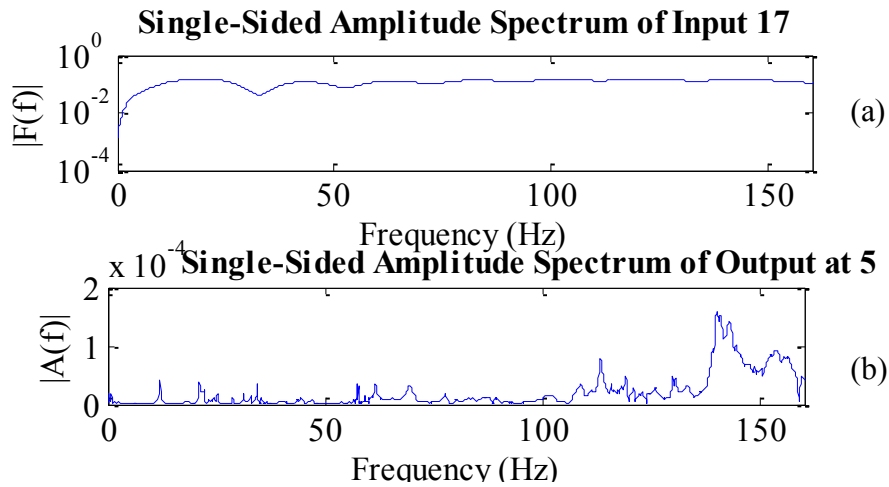
Figure 5.24. TT frequency domain (a) windowed input and output accelerations

5.3.3 Frequency Response Function and Coherence

As mentioned in the previous chapter, the field test consisted of 20 input locations making the

FRF a 20-by-20 matrix for both the hammer and shaker. Figure 5.25 represents a comparison of

the hammer and shaker at location five, when the input was at location one Besides the lower

frequencies, the FRFs are close in magnitude and identify the modes at near the same

frequencies. The coherences (defined in Section 5.2.3) however, are completely different. The

hammer has a coherence of one at majority of the frequencies except between 0 and 10 Hz. The

shaker coherence values appear to be a lot worse than the sledge hammer. Nonetheless, when

closely examining the peaks of the FRF and determining the corresponding coherence, many of

these values were close to unity. The poor coherence may be due to the input force failing to

overcome noise in the structure. The sledge hammer was able to excite the bridge at 4000 lbs. or

more, but the shaker could only produce 250-300 lbs. Which may be the reason why the

hammer coherence is much better.
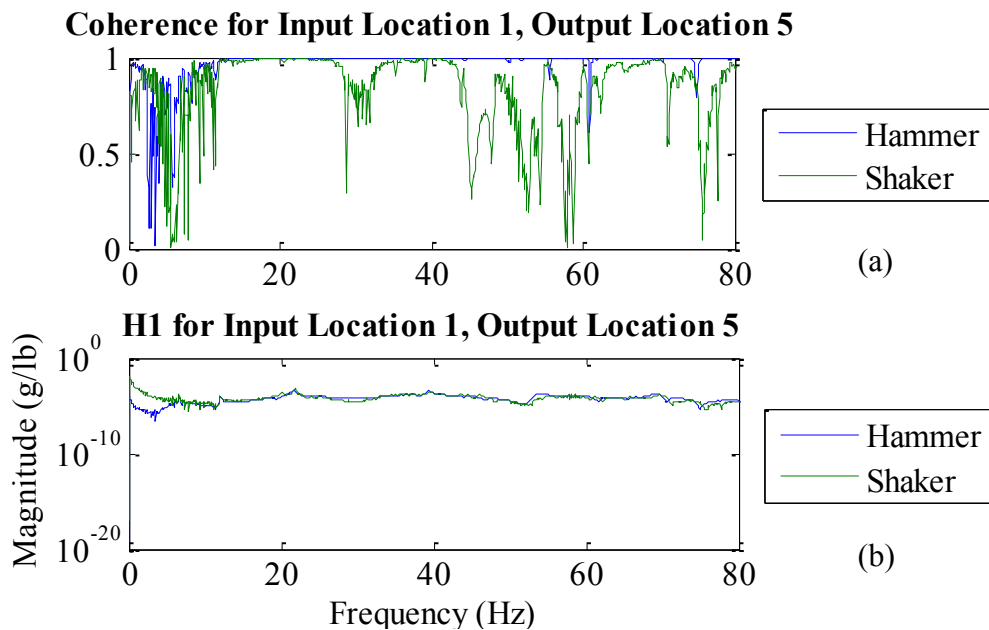
Figure 5.25. Hammer and TT comparison of (a) Coherence and (b) FRF

Coherence for Input Location 13, Output Location 14

Hammer
Shaker

(a)

H1 for Input Location 13, Output Location 14

Hammer
Shaker

(b)
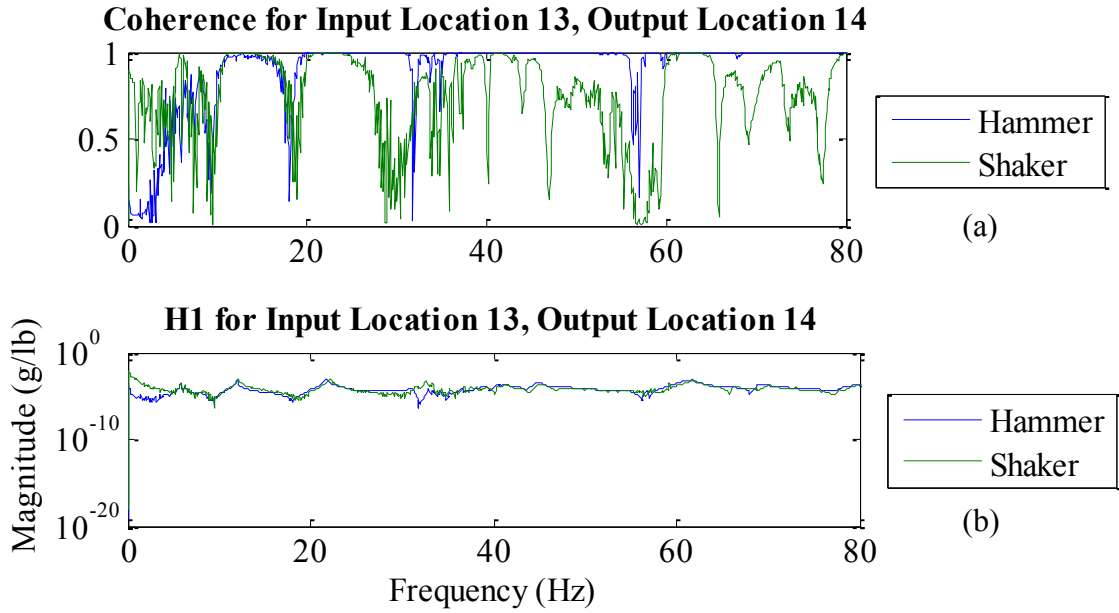
Figure 5.26. Input at DOF 13, Output at DOF 14 (a) Coherence and (b) FRF

Coherence for Input Location 5, Output Location 10

(a)

H1 for Input Location 5, Output Location 10

(b)
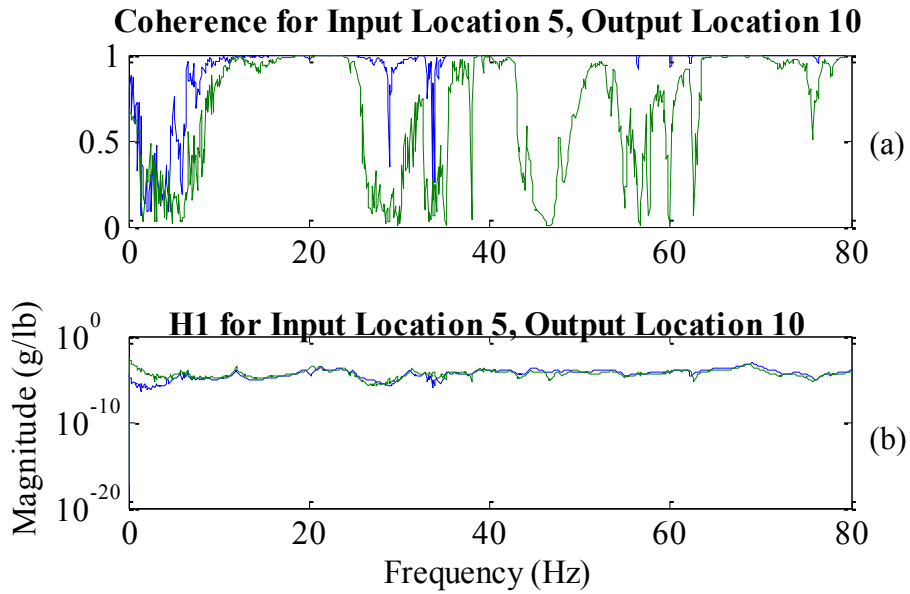
Figure 5.27. Input at DOF 5, Output at DOF 10 (a) Coherence and (b) FRF

Coherence for Input Location 10, Output Location 5

(a)

H1 for Input Location 10, Output Location 5

(b)
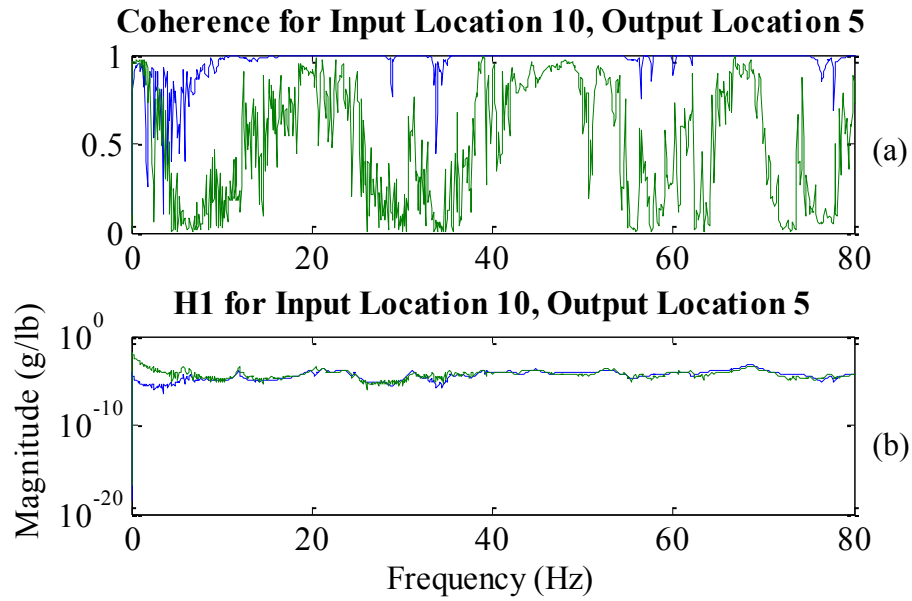
Figure 5.28. Input at DOF 10, Output at DOF 5 (a) Coherence and (b) FRF

Single-Sided Amplitude Spectrum of Input at 5

Single-Sided Amplitude Spectrum of Output 10
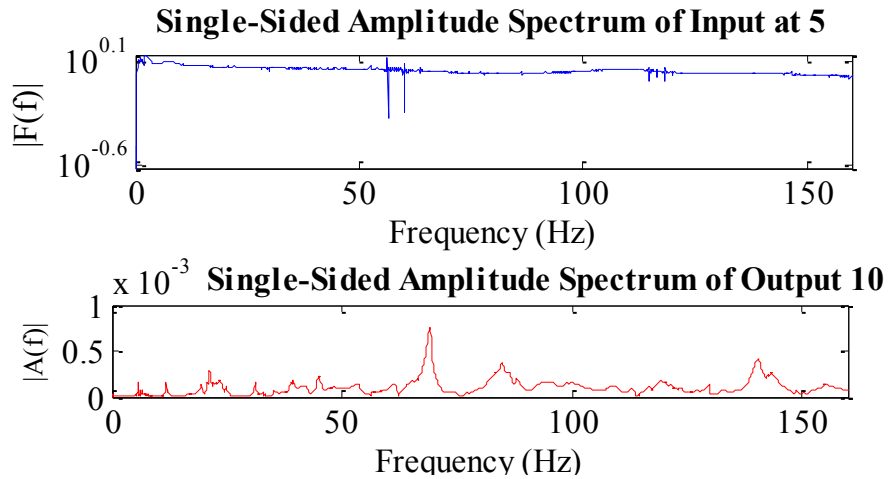
Figure 5.29. FFT of hammer impact using one average at Input 5

Single-Sided Amplitude Spectrum of Input at 10
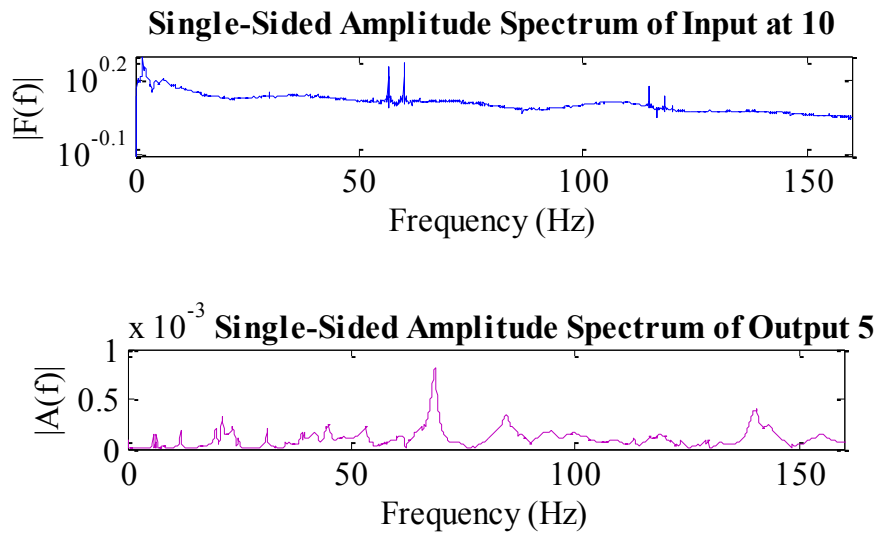
Figure 5.30. FFT of hammer impact using one average at Input 10

Single-Sided Amplitude Spectrum of Input at 5
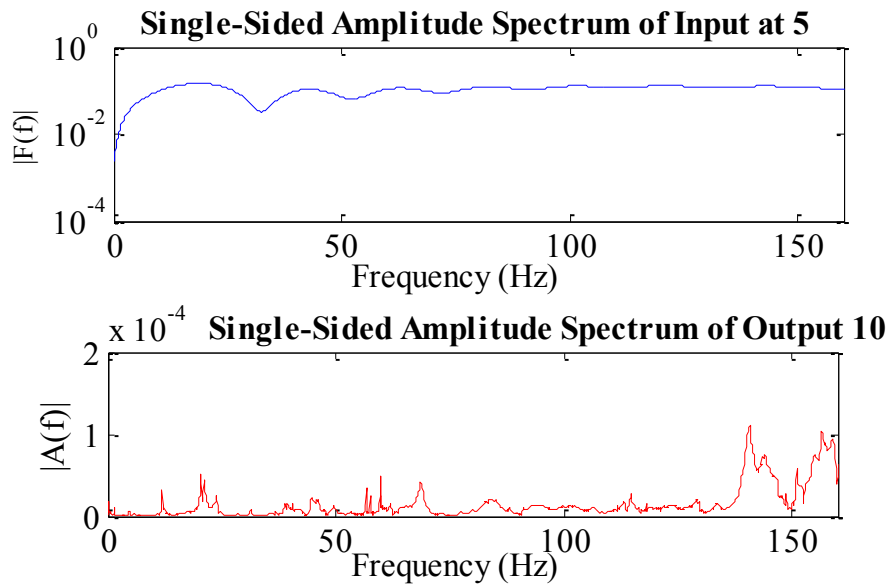
Figure 5.31. FFT of shaker impact using one average at Input 5
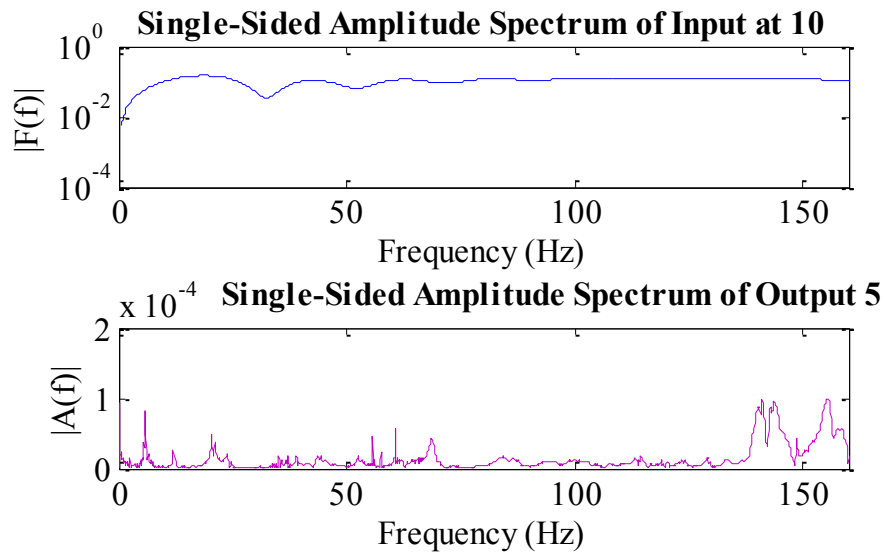
Figure 5.32. FFT of shaker impact using one average at Input 10

Input at location thirteen is shown in Figure 5.26. Unfortunately this location and the majority of

others bear similar results. In Section 5.3.1, applying a force window was mentioned. After

processing the shaker test data without any windowing, the researchers thought it may improve

the coherence. After doing this, the coherence did improve slightly but not to the desired level.

Symmetry is another characteristic that should be displayed by a linearly, time invariant system.

For instance, the response at Degree of Freedom (DOF) 10 due to input at DOF 5 should be

equal or close to the response at DOF 5 due to input at DOF 10. This can be checked by

examining the FRF values and/or figures. Figure 5.27 and Figure 5.28 show very similar FRFs

in the bottom half of the figures. The peaks are seen in the same location and have similar

magnitudes. Since, compiling the FRF requires adding several averages together, the values may

be slightly different. The FFT of one impact at DOFs five and ten were inspected as well for

close symmetry. This comparison for the hammer is seen in Figure 5.29 and Figure 5.30 . The

input forces may not look similar, depending on the quality of the impacts, but the response

should. The hammer displays this characteristic. The shaker comparison in Figure 5.31 and

Figure 5.32 is not exactly symmetrical but close.

5.3.4 Modal Analysis Discussion
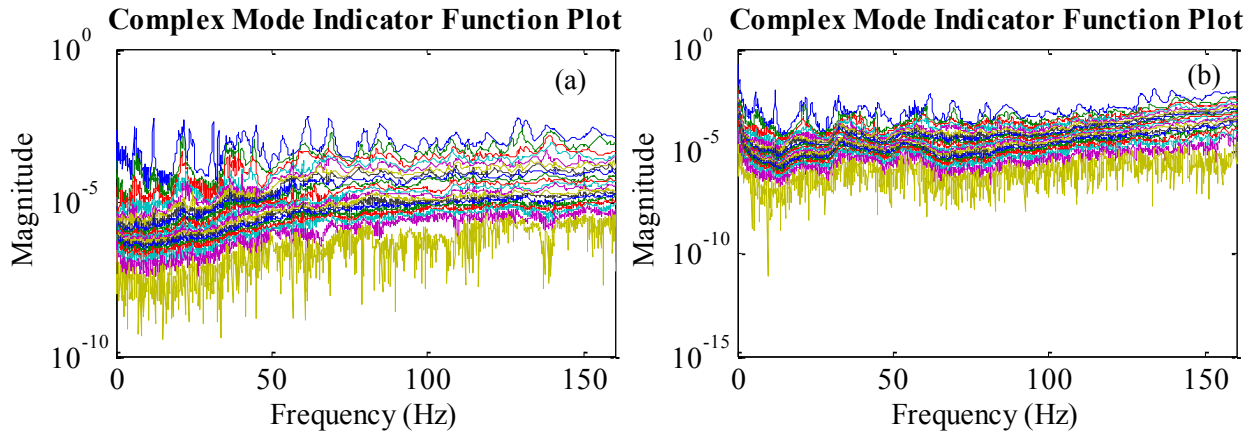
Figure 5.33. CMIF plots of (a) hammer (b) shaker

Although, coherence was subpar using the tactile transducer, both methods of testing were able

to identify the majority of the modes associated with the bridge. The Complex Mode Indicator

Function was used to display peaks that are estimates of mode shapes. Similar to the laboratory

results, these figures do not resemble the typical CMIF plot. Each curve of the plot represents a

singular value computed during Singular Value Decomposition. There were 16 modes identified

using the hammer and 15 using the tactile transducer.
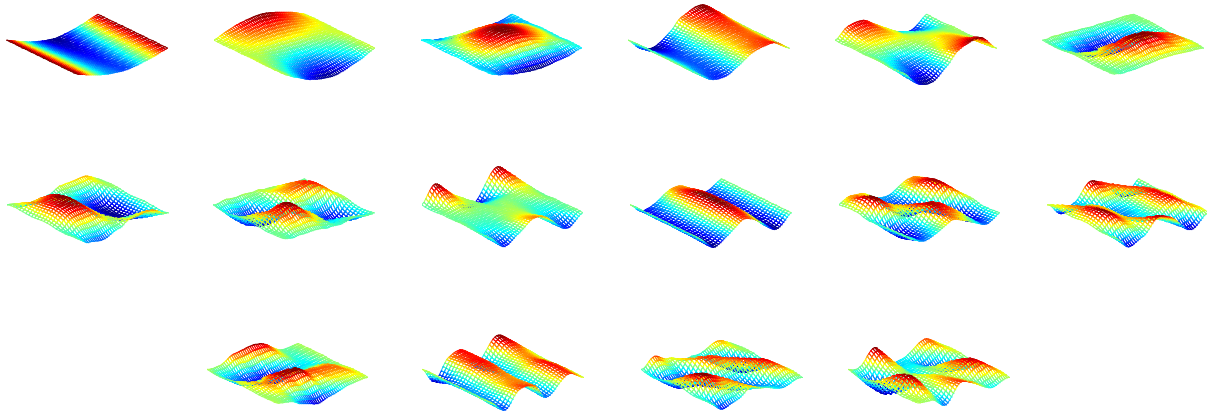
Figure 5.34. Hammer mode shape plots
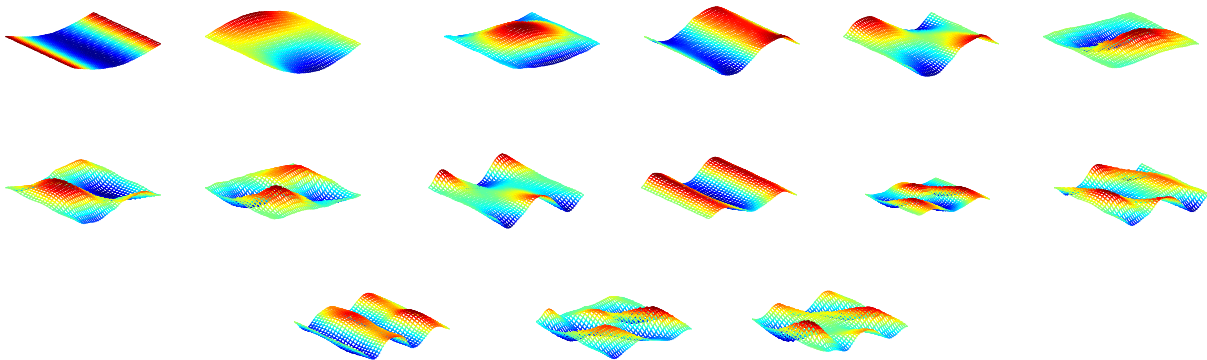
Figure 5.35. Shaker mode shape plots

Figure 5.34 and Figure 5.35 show the mode shapes identified by each of the methods. The frequency, damping ratio, and description of each mode shape is in Table 5.5 and Table 5.6. When using the sledge hammer during the field test, the goal was to get ten good impacts whereas with the hammer twenty were needed. For the hammer, modal parameters were analyzed based on three, five, seven and ten averages. Five, ten, fifteen, and twenty averages were considered when deriving the modal parameters from the tactile transducer test. The properties in Table 5.5 from the hammer are based on ten averages and those in Table 5.6 are from 20 averages. Of the 16 modes identified using the hammer, five did not have a description name. These are either anti-symmetric or local modes. By looking at the frequencies that were

found, one can see that some of these modes were found very close to other modes. Damping values do not reflect a consistent or proportional change in any manner. The same pattern can be seen with the shaker data, except that Mode 13 was not found at all.

Table 5.5. Identified modal parameters via sledge hammer

Mode	Frequency	Damping	Description
1	5.80	1.08	Bending 1
2	6.54	0.87	Torsion 1
3	11.91	0.78	Butterfly 1
4	20.12	1.30	Bending 2
5	21.22	1.13	Torsion 2
6	21.83	0.73	-------------
7	24.91	1.39	Butterfly 2
8	32.86	0.16	-------------
9	36.17	1.38	Torsion 3
10	38.99	1.30	Bending 3
11	47.36	1.19	-------------
12	54.51	2.22	Butterfly 3
13	56.44	0.05	-------------
14	63.97	2.00	Bending 4
15	65.35	0.30	-------------
16	77.12	0.57	-------------

Table 5.6. Identified modal parameters via tactile transducer

Mode	Frequency	Damping	Description
1	5.98	0.10	Bending 1
2	6.53	0.89	Torsion 1
3	12.00	0.81	Butterfly 1
4	20.40	0.83	Bending 2
5	21.36	2.14	Torsion 2
6	22.08	0.70	-------------
7	25.13	0.65	Butterfly 2
8	32.61	0.22	-------------
9	36.00	2.18	Torsion 3
10	39.19	1.44	Bending 3
11	47.27	0.97	-------------
12	53.63	1.03	Butterfly 3
13	-------------	-------------	-------------
14	64.41	0.86	Bending 4
15	65.95	0.58	-------------
16	77.62	0.36	-------------

A comparison of frequencies and damping ratios found with varying averages is shown in Figure 5.36 for the sledge hammer and Figure 5.37 for the tactile transducer. The frequencies for each mode are consistently identified for all varying amounts of averages using the hammer and tactile transducer. Mode 13, which could not be given a description name based on its shape, is the only frequency left to question when considering frequencies found by the shaker. On the other hand, damping could not be consistently captured by the hammer or shaker. Considering the hammer modal comparison figure along with Table 5.7, the mode with the least varying damping values is Mode 8 which also could not be named based on the shape. Mode 12, which is Butterfly 3, had damping values that deviated the most from the mean. For the shaker, Table 5.8 helps depict the inconsistent variations captured by the shaker. Mode 6 had damping values that deviated the least from the mean. This mode also could not be given a description. Bending 4 (Mode 14) contained the highest damping variations. The use of 20 averages identified the lowest damping value of 0.86% and the highest, 2.04 which was identified using five averages.

It was noted that during data processing it was difficult to identify Bending 4 and Butterfly 4.

Often times, when using the CMIF plot, the sharpest peak is identified as a mode. However,

smaller peaks to the left and right, if chosen, will also identify the mode. These peaks can be

referred to as "pages" within the FRF. With Bending 4, the exact page had to be used each time.

In structures with less than 10% damping, small errors in estimation of the poles during eFRF

computation can lead to large distortions and fluctuations in damping (Fernstrom, 2014). Since

the hammer, had less variations in damping and smaller range for the confidence interval, it was

considered the more accurate method for damping when determining the percent error.

Disregarding Mode 13, the range of error was anywhere from 1.015% to 62% when using five

averages. With ten averages, this range was from 2.065% to 80.09%.
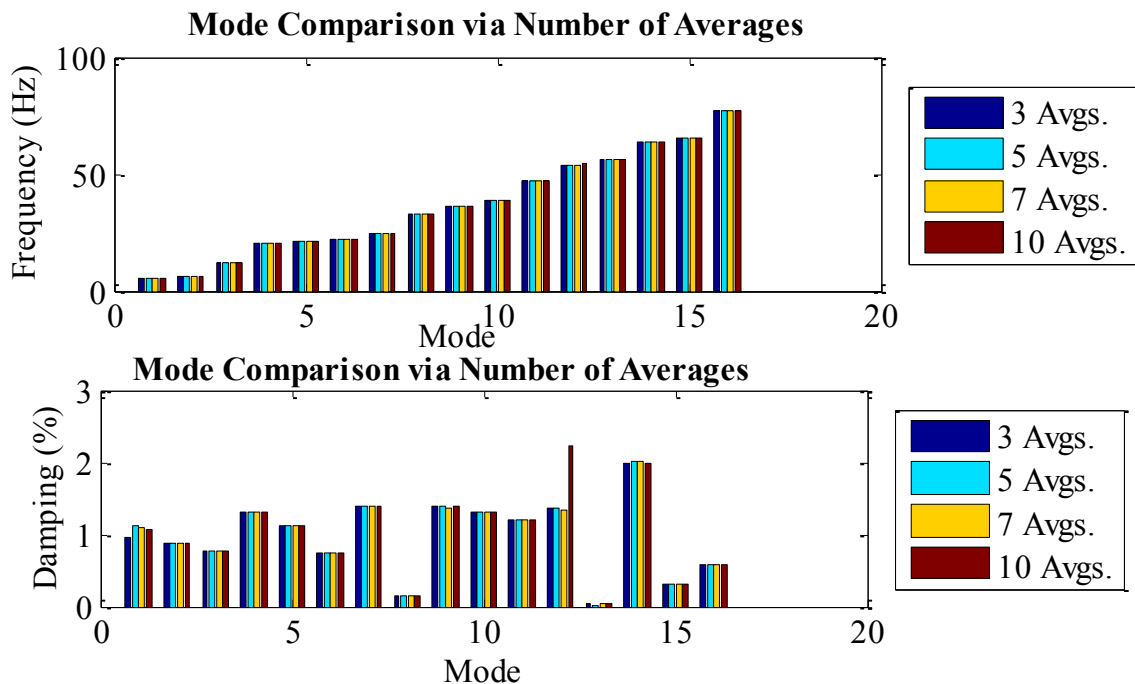
Figure 5.36. Hammer modal comparison

Mode Comparison via Number of Averages
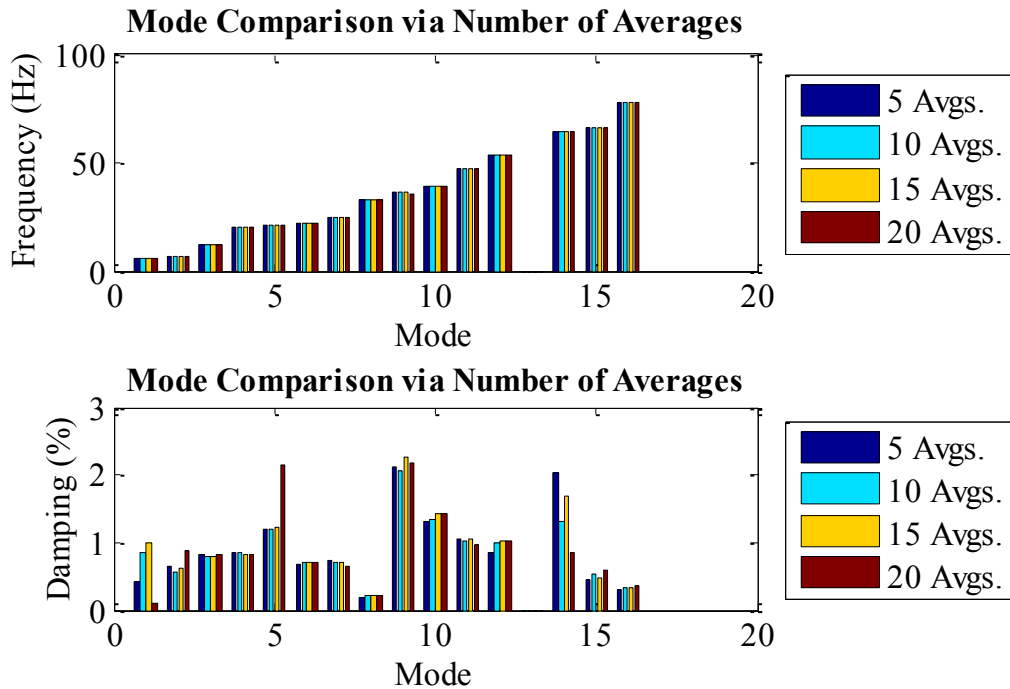
Figure 5.37. Shaker modal comparison

Table 5.7. Hammer damping ratio descriptive statistics

Mode	3 Avgs.	5 Avgs.	7 Avgs.	10 Avgs.	Mean	Std. Dev.	C.I.-95%
1	0.97	1.13	1.09	1.08	1.068	0.068	0.108
2	0.89	0.88	0.88	0.87	0.880	0.012	0.019
3	0.77	0.77	0.77	0.78	0.772	0.008	0.012
4	1.31	1.31	1.31	1.30	1.307	0.004	0.006
5	1.13	1.13	1.13	1.13	1.131	0.002	0.003
6	0.73	0.73	0.73	0.73	0.732	0.001	0.002
7	1.39	1.39	1.39	1.39	1.388	0.003	0.005
8	0.16	0.16	0.16	0.16	0.164	0.000	0.001
9	1.39	1.38	1.37	1.38	1.377	0.009	0.014
10	1.30	1.31	1.31	1.30	1.306	0.003	0.005
11	1.19	1.19	1.19	1.19	1.190	0.002	0.004
12	1.36	1.36	1.35	2.22	1.572	0.435	0.692
13	0.05	0.02	0.04	0.05	0.043	0.014	0.022
14	2.00	2.02	2.02	2.00	2.010	0.012	0.018
15	0.30	0.30	0.30	0.30	0.297	0.001	0.001
16	0.57	0.57	0.57	0.57	0.569	0.001	0.001

Table 5.8. Shaker damping ratio descriptive statistics

Mode	5 Avgs.	10 Avgs.	15 Avgs.	20 Avgs.	Mean	Std. Dev.	C.I.-95%
1	0.42	0.84	0.985	0.10	0.586	0.403	0.642
2	0.65	0.574	0.614	0.89	0.680	0.140	0.223
3	0.81	0.800	0.793	0.81	0.805	0.010	0.016
4	0.84	0.839	0.836	0.83	0.837	0.004	0.007
5	1.21	1.210	1.227	2.14	1.445	0.462	0.736
6	0.69	0.701	0.699	0.70	0.698	0.003	0.004
7	0.73	0.720	0.702	0.65	0.699	0.035	0.056
8	0.18	0.212	0.213	0.22	0.207	0.015	0.024
9	2.11	2.066	2.269	2.18	2.157	0.088	0.141
10	1.30	1.333	1.432	1.44	1.377	0.069	0.109
11	1.06	1.030	1.049	0.97	1.028	0.039	0.062
12	0.86	1.007	1.018	1.03	0.978	0.082	0.130
13	----------	----------	----------	----------	----------	----------	----------
14	2.04	1.31	1.69	0.86	1.476	0.509	0.810
15	0.44	0.53	0.48	0.58	0.508	0.059	0.095
16	0.30	0.32	0.32	0.36	0.325	0.024	0.038

MAC is another approach to determine how correlated hammer and tactile transducer values are. These values were found using Equation 5.17 as well. For the field test, two MAC computations were completed. The first was to compare ten averages of the hammer to ten averages of the shaker. The next compared ten averages of the hammer to twenty averages of the shaker. Majority of the MAC values in Figure 5.38 along the diagonal are close to one except for Mode 5 (Torsion 2), Mode 13, Mode 14 (Bending 4), and Mode 16. Mode 5 is the lowest with 0.3496, followed by Mode 16 with 0.8084 and then Mode 14 with 0.9012. Since Mode 13 was not found using the tactile transducer, this resulted in a value of zero. Figure 5.39 shows that a much better correlation between the two methods is achieved when more averages are used in data processing for the shaker. The last three modes are still slightly lower than expected, but have better agreement than using only ten averages from the shaker test.

Hartbarger Modal Assurance Criterion (MAC)
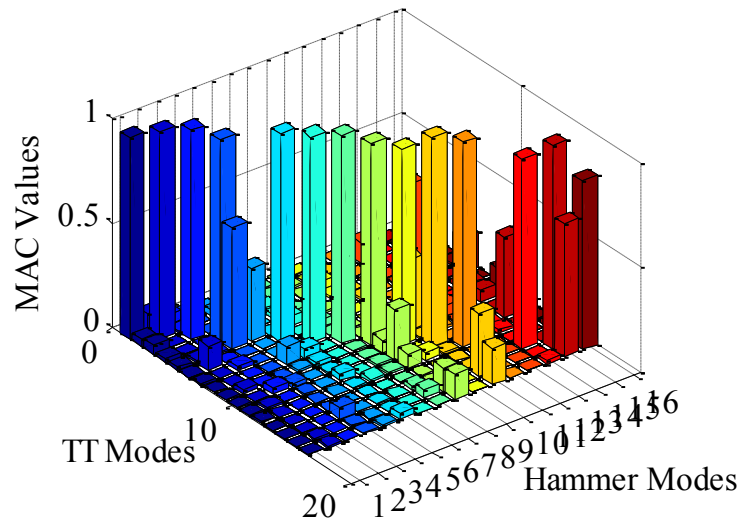
Figure 5.38. MAC: 10 hammer averages vs. 10 shaker averages

Hartbarger Modal Assurance Criterion (MAC)
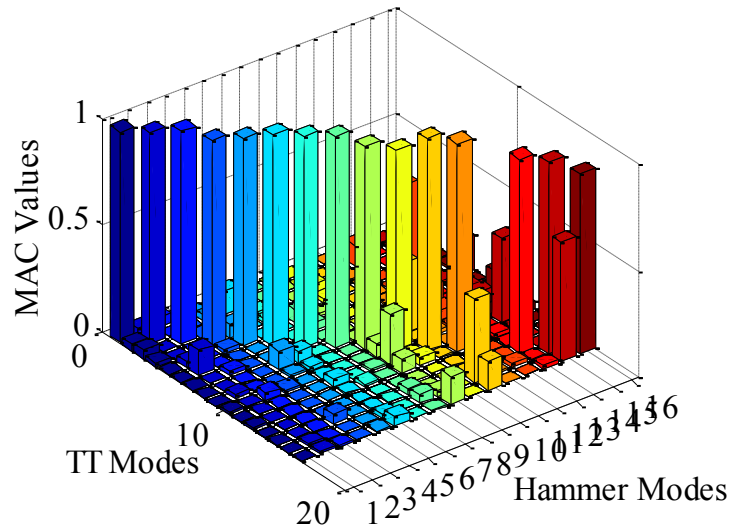
Figure 5.39. MAC: 10 hammer averages vs. 20 shaker averages

The eFRFs representing the hammer and shaker can be seen in Figure 5.40 and Figure 5.41 respectively. Mode 1 and 2 are shown in these figures. Considering the eFRFs of the laboratory tests, both methods used in the field are much noisier. Additionally, the overlay (thick black curve) do not fit as well as expected. However, the hammer synthesized eFRFs prove to agree

better with the actual FRF than that of the tactile transducers. Enhanced Frequency Response

Functions with subpar or questionable agreement are due to actual modes that are poorly

identified or false modes. Poor identification of a mode is caused by either inadequate filtering,

low excitation or excessive noise (Fernstrom, 2014). As mentioned before, the sledge hammer

was able to input much more force than the shaker without over-ranging accelerometers. This

could be the reason for better modal synthesis with the hammer.
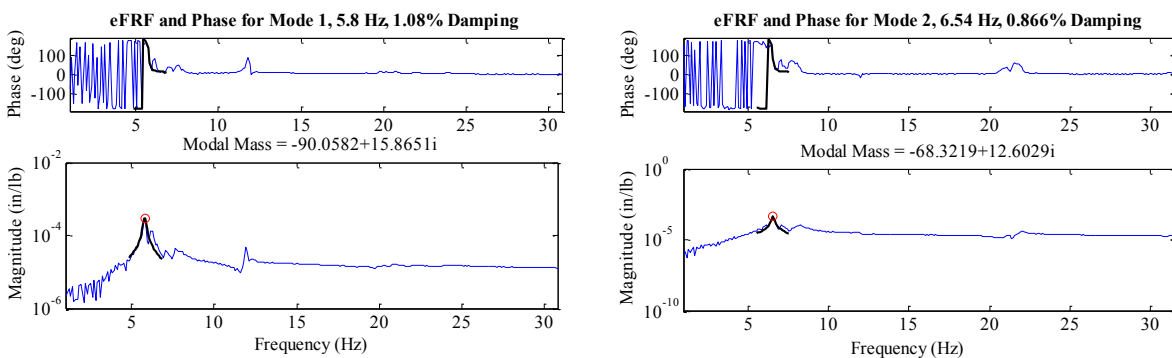
Figure 5.40. Hammer Enhanced Frequency Response Functions
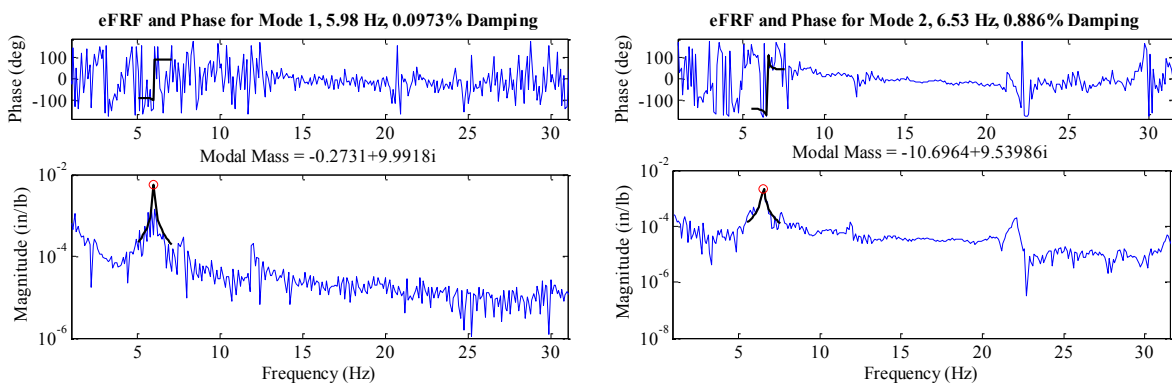
Figure 5.41. Shaker Enhanced Frequency Response Functions

5.3.5 Comparison to Previous Impact Test Completed By Others

Previous testing of Hartbarger Bridge was completed by several other graduate students at the

University of Arkansas. Modal parameters of these tests will be compared to the findings from

the sledge hammer and tactile transducer tests. A brief description of the tests considered are described in the following sections (Fernstrom, 2014).

Multisine MIMO was completed by Eric Fernstrom in September 2013.
Output DOFs: 20
Frequency resolution: 0.04 Hz
Frequency Range: 4-70 Hz
Weather: Sunny, humid, very few clouds, 75-85 ºF

Ryan Maestri performed Ambient 1 on December 10, 2010
Output DOFs: 24
Frequency resolution: 0.024 Hz
Weather: 45˚F, sunny, calm winds, low humidity

Javier Torres completed Ambient 2 on November 14, 2011
Output DOFs: 28
Frequency resolution: 0.0305 Hz
Weather: 40˚F, clouds, calm winds, low humidity

Impact 1 was done by Jeremy Rawn on November 5, 2010
Output DOFs: 16
Frequency resolution: 0.0625 Hz
Weather: 60˚F, sunny, calm winds, low humidity
Three impacts per DOF

Javier Torres performed Impact 2 on November 14, 2011
Output DOFs: 28
Frequency resolution: 0.00098 Hz
Weather: 40˚F, clouds, calm winds, low humidity
Five impacts per DOF

Table 5.9 and Table 5.10 contain the modal parameters that were identified via the tests described above. To determine how close the current testing methods are to previous impact tests, Table 5.11 and Table 5.12 are used to show error when comparing the natural frequencies of Impact 1 and Impact 2. There are modes from each different test that has modes not identified by the other impact tests. The frequencies were matched up as close as possible. For Impact 1, the frequencies that did match, had an error no larger than ten percent. This is true for both the shaker and hammer. The same can be said for each of the modes for Impact 2 except number 19.

The error relative to the hammer is 13.71% and the shaker 14.44%. Unfortunately, damping

values were not as consistent. Similar to comparison with different varying averages, damping

errors do not have a pattern and cannot be predicted (Table 5.13 and Table 5.14). It is

noteworthy to mention, all of the previous tests were performed on the second span of the bridge

whereas the research herein was performed on the third. This is the reason for some of the

differences in natural frequencies and damping.

Table 5.9. Natural frequencies found by previous tests;* Mode not found (Fernstrom, 2014).

Mode	MS	Ambient	Ambient	Impact	Impact
1	6.12	6.03	6.04	6.10	6.02
2	6.98	7.03	7.02	7.04	6.94
3	12.21	12.38	12.39	12.50	12.46
4	21.69	22.09	*	21.67	21.60
5	22.48	*	*	23.35	23.45
6	22.71	*	22.71	22.81	22.61
7	24.32	24.59	25.57	24.57	24.37
8	32.18	32.25	32.50	32.46	32.48
9	34.04	*	34.21	*	34.19
10	36.07	*	36.50	36.34	*
11	40.54	40.55	41.50	*	40.34
12	46.02	*	45.53	46.47	*
13	48.00	*	*	*	48.47
14	50.56	*	*	51.72	51.30
15	52.12	*	*	*	*
16	54.77	*	56.15	55.88	56.86
17	62.26	*	63.69	63.74	64.25
18	65.47	*	*	*	*
19	67.74	*	*	*	67.82

Table 5.10. Damping ratios found by previous tests; * Mode not found (Fernstrom, 2014).

Mode	MS MIMO	Ambient 2	Impact 1	Impact 2
1	0.59	0.75	0.80	0.44
2	0.89	1.02	0.91	0.98
3	0.78	1.06	0.76	0.70
4	0.76	*	2.29	1.80
5	0.98	*	0.64	0.52
6	0.80	1.76	1.20	0.89
7	0.90	0.75	0.97	1.16
8	0.42	0.37	0.36	0.38
9	0.21	0.19	*	0.11
10	0.17	0.17	0.24	*
11	0.70	0.37	*	0.73
12	1.06	0.51	1.23	*
13	0.74	*	*	0.67
14	0.77	*	0.91	0.98
15	0.57	*	*	*
16	1.03	1.24	1.25	0.88
17	0.54	0.32	0.58	0.48
18	1.60	*	*	*
19	0.34	*	*	0.30

Table 5.11. Natural frequency percent error comparison to Impact 1

Mode	Impact 1	Hammer	Percent	Shaker	Percent
1	6.1	5.80	4.97	5.98	1.89
2	7.04	6.54	7.13	6.53	7.21
3	12.5	11.91	4.69	12.00	4.04
4	21.67	20.12	7.15	20.40	5.86
5	23.35	21.22	9.11	21.36	8.54
6	22.81	21.83	4.32	22.08	3.20
7	24.57	24.91	1.36	25.13	2.29
8	32.46	32.86	1.24	32.61	0.48
9					
10	36.43	36.17	0.71	36.00	1.18
11		38.99		39.19	
12	46.47	47.36	1.92	47.27	1.71
13					
14	51.72	54.51	5.39	53.63	3.69
15					
16	55.88	56.44	1.01		100.00
17	63.74	63.97	0.36	64.41	1.05
18		65.35		65.95	
19		77.12		77.62	

Table 5.12. Natural frequency percent error comparison to Impact 2

Mode	Impact 2	Hammer	Percent	Shaker	Percent
1	6.02	5.80	3.710369	5.98	0.582336
2	6.94	6.54	5.79354	6.53	5.87783
3	12.46	11.91	4.385589	12.00	3.72776
4	21.6	20.12	6.845469	20.40	5.555367
5	23.45	21.22	9.49361	21.36	8.932947
6	22.61	21.83	3.47076	22.08	2.347196
7	24.37	24.91	2.196256	25.13	3.127888
8	32.48	32.86	1.173918	32.61	0.413238
9	34.19		100		100
10		36.17		36.00	
11	40.34	38.99	3.350629	39.19	2.861216
12					
13	48.47	47.36	2.288975	47.27	2.484238
14	51.3	54.51	6.256396	53.63	4.534795
15					
16	56.86	56.44	0.735703		100
17	64.25	63.97	0.434703	64.41	0.248133
18		65.35		65.95	
19	67.82	77.12	13.71846	77.62	14.44889

Table 5.13. Damping ratio percent error comparison to Impact 1

Mode	Impact 1	Hammer	Percent	Shaker	Percent
1	0.8	1.08	35.04	0.10	87.84
2	0.91	0.87	4.82	0.89	2.68
3	0.76	0.78	3.12	0.81	7.00
4	2.29	1.30	43.07	0.83	63.72
5	0.64	1.13	76.45	2.14	234.13
6	1.2	0.73	38.98	0.70	41.84
7	0.97	1.39	43.30	0.65	33.21
8	0.36	0.16	54.23	0.22	39.57
9					
10	0.24	1.38	473.05	2.18	808.89
11		1.30		1.44	
12	1.23	1.19	3.03	0.97	20.95
13					
14	0.91	2.22	144.43	1.03	13.24
15					
16	1.25	0.05	95.87		100.00
17	0.58	2.00	245.36	0.86	47.79
18		0.30		0.58	
19		0.57		0.36	

Table 5.14. Damping ratio percent error comparison to Impact 2

Mode	Impact 2	Hammer	Percent	Shaker	Percent
1	0.44	1.08	145.53	0.10	77.89
2	0.98	0.87	11.62	0.89	9.64
3	0.7	0.78	11.96	0.81	16.17
4	1.8	1.30	27.57	0.83	53.84
5	0.52	1.13	117.17	2.14	311.23
6	0.89	0.73	17.73	0.70	21.58
7	1.16	1.39	19.83	0.65	44.15
8	0.38	0.16	56.63	0.22	42.75
9	0.11		100.00		100.00
10		1.38		2.18	
11	0.73	1.30	78.41	1.44	96.99
12					
13	0.67	1.19	78.01	0.97	45.12
14	0.98	2.22	126.97	1.03	5.15
15					
16	0.88	0.05	94.14		100.00
17	0.48	2.00	317.31	0.86	78.58
18		0.30		0.58	
19	0.3	0.57	90.09	0.36	18.92

5.3.6 Modal Flexibility

As stated before, modal flexibility is a square matrix that is the size of the number of DOFs. To plot modal flexibility, a unit load is applied to each DOF which then yields a deflection profile. Views of the hammer modal flexibility profile can be seen in Figure 5.42. Flexibility due to the ten averages using the tactile transducer is represented in Figure 5.43 and twenty averages are in Figure 5.44. Despite ten averages providing a smoother, cleaner profile, twenty averages provides values closer to those of the hammer. Percent error and the Frobenius Norm calculations (Fernstrom, 2014) were completed to compare modal flexibility matrices. Frobenius norm calculations were completed using the main diagonals of the two flexibility matrices, D_d and all terms of the matrices, D. Comparing ten averages of the hammer to twenty averages of

the shaker yielded better results than the comparison with ten averages of the shaker. The

diagonal comparison with twenty shaker averages yielded a value of 2.2 whereas the complete

matrix comparison was 494.4. The D_d value of ten averages was 33.71 and the D value was

10717.30. The D values show that some error occurred when estimating modal vectors.

Considering percent error, some values throughout the matrices had reasonable error. Others

were far above 100% due to major estimation error. However, to reduce error in the modal

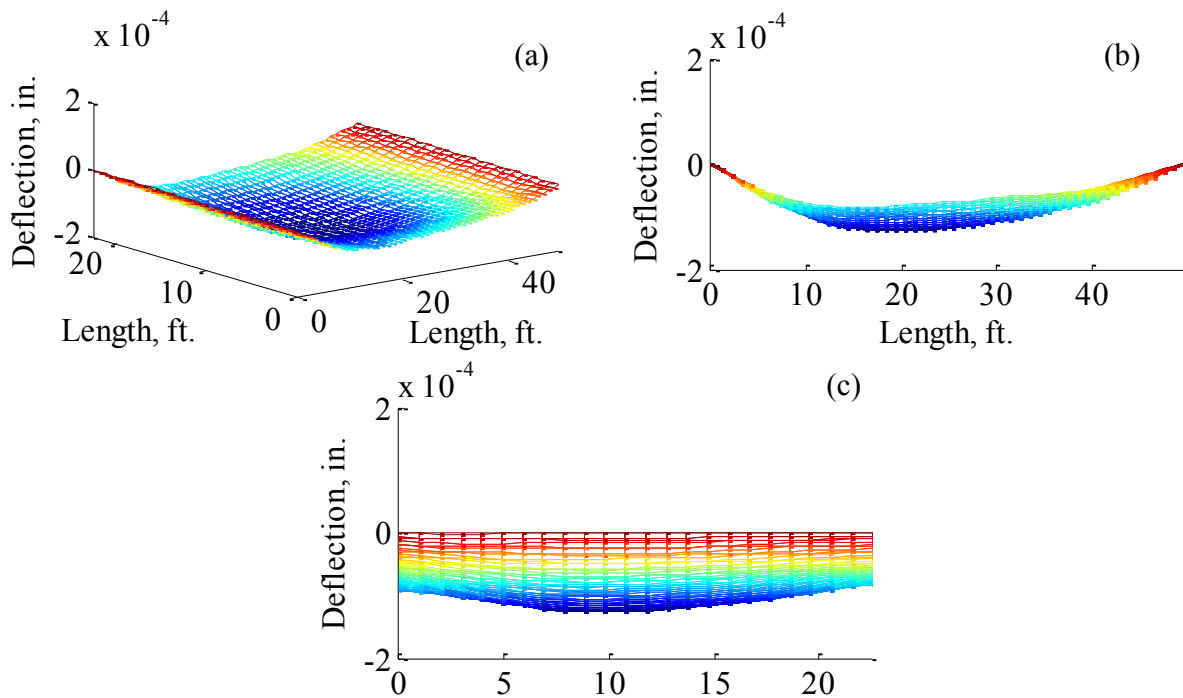flexibility matrix, more averages using the shaker are needed.

Figure 5.42. Hammer modal flexibility (10 Avgs.): (a) 3D View, (b) Side View, and (c) End View
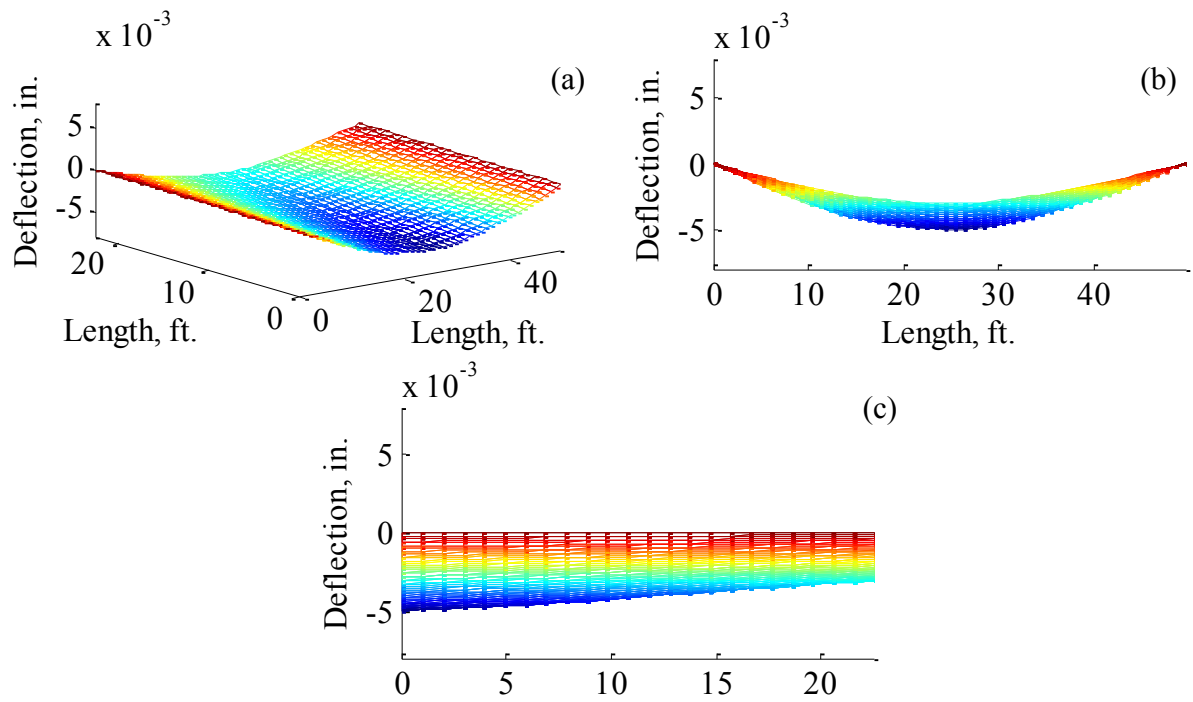
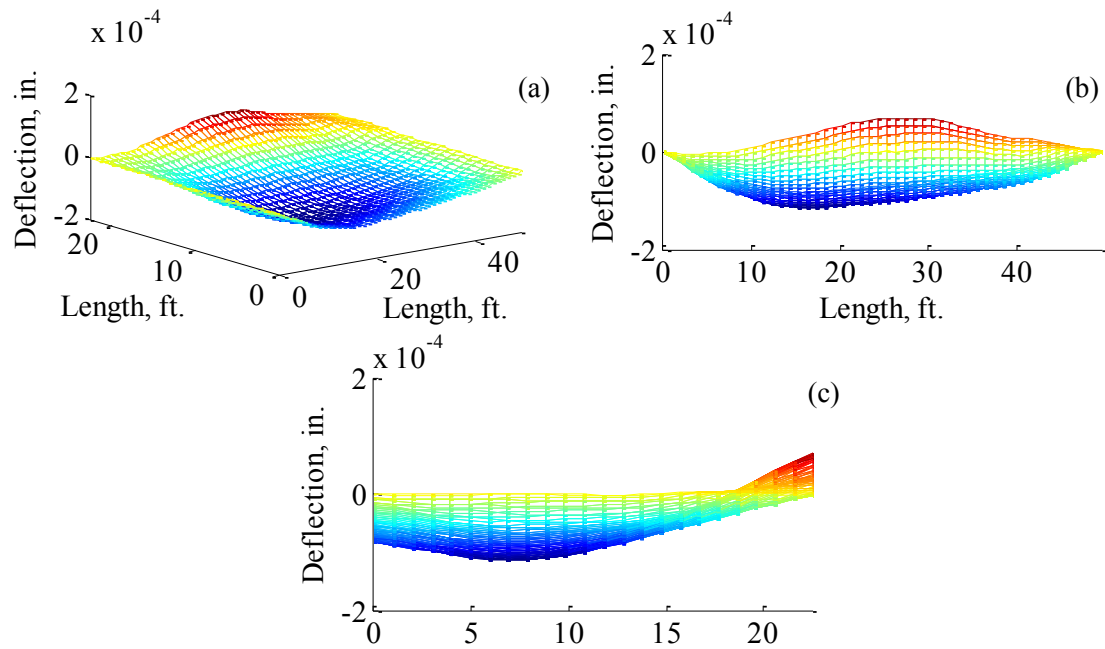**Figure 5.43. Shaker modal flexibility (10 Avgs): (a) 3D View, (b) Side View, and (c) End View**

Figure 5.44. Shaker modal flexibility (20 Avgs.): (a) 3D View, (b) Side View and (c) End View

CHAPTER SIX

CONCLUSIONS AND RECOMMENDATIONS

6.1 LABORATORY TESTING PROGRAM

Laboratory testing allowed for researchers to see how each device performed in a controlled environment with minimal temperature variation and noise effects. Each device was able to produce a force anywhere between 50-100 lbs. that adequately excited the structure. The input force is the most notable difference between the two testing methods. While the hammer was able to create a sharp peak, the tactile transducer consisted of a free decay. Despite this difference, the response spectrum was the same and twelve clear modes were identified using each device. Modes of the grid structure were easily identified and coherence at most frequencies were close to unity. Overall, the shaker displayed better coherence than the hammer. Between the two methods, majority of the modes were close in frequency. Some of the later modes were further spaced apart. Both were able to accurately identify twelve mode shapes. MAC values show that the modal vectors agree. As far as damping, one method cannot be deemed better than the other. After filtering and synthesizing of modes, not all eFRFs had a sharp narrow peak but all overlays did fit the original FRF; this is true using the impact hammer and tactile transducer. Modal flexibility was somewhat different using the two methods. This is due to some bad quality estimates at some of the DOFs. The number of averages used to compile the FRF only proved to have a major effect on the damping ratios found. However, as far as lab testing, the shaker does prove to be just as adequate as the shaker.

6.2 FIELD TESTING PROGRAM

Field results seemed to be opposite that of the laboratory results. Using the hammer on the top side of the bridge allowed for a much larger force to be input on the structure. This ranged anywhere from 3500-5000 lbs. Even though the input forces looked the same as those from the laboratory study, it was necessary to apply a force window on the shaker data to improve coherence of the FRF. Unlike the laboratory test, the shaker had much more poor coherence. The shaker was only able to identify 15 of the 16 total modes found. Modes were not easily identified in either method which is probably due to noise of the bridge. The natural frequencies of both methods are comparable but damping still remains a major issue. Comparing MAC values were affected by the number of averages used with the tactile transducer. There were several aspects that could have distorted the measurements of the shaker. Such as, loosening of bolts, vibrating of the structure before and after a vehicle reached the bridge, and exciting the structure at an inadequate force level. The shaker test took about four hours longer than the hammer test. This is because only one shaker was used and had to be moved after each input location was completed. With 3-5 shakers, this process may have been quicker than the hammer test. The shaker is adequate in estimating the natural frequencies of the structure. At this time, considering damping ratios, neither method can be judged better than the other. However, when using the tactile transducer, more averages are needed to get better agreement between MAC values and modal flexibility. Diagonals of the modal flexibility matrices agreed well but the overall matrices did not. As said before this is due to some of the DOFs having identified one or two modes that may not be the same shape.

6.3 SUMMARY CONCLUSIONS

As mentioned previously, the tactile transducer was able to adequately identify the natural frequencies and modal flexibilities of the laboratory and field structures. Additionally, when comparing the modal vectors of the two different testing methods, MAC values displayed sufficient agreement for both the laboratory and field test. Several other characteristics of the shaker test were observed and used to draw conclusions. They are listed below.

- TT input force generated in the field was significantly lower force than hammer force
  - More critical issue for field test since the structure was more massive
  - Generated force was limited by the available data acquisition equipment (±5 V input range)
  - Caused a low signal-to-noise ratio
- More averages required due to a lower signal-to-noise ratio
  - Variation in force due to friction
- TT impulse not as clean as hammer
  - TT continues to vibrate with structure after impact
  - Internal friction of the moving mass before impact needs to be filtered
  - Force transducers read the unwanted operational mechanics of the TT

6.4 RECOMMENDATIONS

 For future use of the tactile transducer as an impact device, it is necessary to figure out a way to get better coherence in the field. Good coherence during the laboratory study leads to the assumption that an aspect of the field structure causes more noise to be present. To effectively use the device as an impact testing alternative, overcoming these noise issues is necessary. Considering the analyzed data, 20 impacts should be the minimum at each DOF. Even though the tactile transducer inputs far more consistent impacts than the hammer, the force level could be much more constant. By having a set input force, the experimenter would always know what force to expect. With that said, the shaker could be programmed to create a force at a specific level and load cells with an appropriate input range (above 300 lbf.) could be used. The current

issue is that each load cell used can only read a maximum of 100 lbf.; totaling to a maximum of 300 lbf. Given the results, this was not an optimal force level for obtaining good signal-to-noise ratio. After acquiring an adequate, constant input force, the dynamics of the tactile transducer itself should be investigated and optimized. Use of several clamps could be eliminated by attaching strong magnets to the bottom of the tactile transducers. As this method becomes more utilized, researchers should consider the use of a completely automated procedure involving wireless sensors and remote monitoring. Remote monitoring would allow for testing to be completed more often with only one setup time.

When attempting to balance three force transducers in order to read equal amounts of force, this could not be accomplished. Each impact created a different reading in the load cells. There was no pattern or way to predict what may happen. It is suspected that the movement inside the tactile transducer is not completely up and down. This will cause sporadic readings each time there is an impact. If this aspect of the device can be perfected, a balanced load cell configuration can be established and two of the load cells can be replaced with studs. Meaning that other load cells can be used on other tactile transducers and less would be needed. With a constant force and balanced load cell setup, researchers could save money on force transducers making the already low cost system even cheaper.

In addition to limitations with the tactile transducer itself, there are certain structural properties that determine whether this device is useable. For instance, since the study was completed on a highway bridge that is representative of a large number of bridges in the United States, it gives insight into a new impact testing method. However, the type of structure that is being considered must be heeded. Use of a tactile transducer is limited to use on short span bridges with natural frequencies ranging from 5-150 Hz. Suspension and cable-stayed bridges are currently outside

of the scope of use for this device. Nevertheless, impact testing using tactile transducers could

be used to evaluate specific components of such bridges including stay cables, suspender cables,

lighting fixtures, railings, etc.

CHAPTER SEVEN

REFERENCES

7.1 REFERENCES

Aktan, A. (1993). Structural identification of a steel stringer bridge. *Transportation Research Record, 1393*, 175-185.

Allemang, R. (2003). The modal assurance criterion- twenty years of use and abuse.*Sound and Vibration, 37*(8), 14-23.

American Society of Civil Engineers. (2013). 2013 report card for America's Infrastructure. (). Reston, VA: American Society of Civil Engineers.

Brownjohn, J. M. W., Dumanoglu, A. A., Severn, R. T., & and Taylor, C. A. (1987). Ambient vibration measurements of the humber suspension bridge and comparison with calculated characteristics. *Proceedings of the Institution of Civil Engineers (London),83*(2), 561-600.

Carreiro, J., Fernstrom, E., & Grimmelsman, K. (2013). Evaluation of low cost dynamic exciters for controlled dynamic testing of bridges. 2013 Structures Congress, ASCE, 422-435.

Catbas, F., Brown, D., & Aktan, A. E. (2004). Parameter estimation for multiple-input multiple-output modal analysis of large structures. *Journal of Engineering Mechanics,130*(8), 921-930.

Coleman, J. (1996). Bridge inspection and assessment - virginia department of transportation. *Structural Materials Technology : An NDT Conference, *, 233-238.

Cunha, A., & Caetano, E. (2006). Experimental modal analysis of civil engineering structures. *Sound and Vibration, 40*(6), 12-20.

Doebling, S. W., & Peterson, L. D. (1997). Computing statically complete flexibility from dynamically measured flexibility. *Journal of Sound and Vibration, 205(5)*, 631-645.

Farrar, C., Duffey, T., Cornwell, P., & Doebling, S. (1999). Excitation methods for bridge structures. *17th International Modal Analysis Conference, * Kissimmee, FL. *, 1* 1063-1068.

Fernstrom, E.V. and Grimmelsman, K.A. (2014). "Comparative Evaluation of Excitation Schemes for Multi-Shaker Testing of Bridges." *Proceedings of the 32nd International Modal Analysis Conference*, Orlando, FL.

Fernstrom, E., Carreiro, J., Rawn, J., & Grimmelsman, K. (2013). Dynamic characterization of a truss bridge by a Falling weight deflectometer. *Transportation Research Record: Journal of the Transportation Research Board, 2331*, 81-89.

Fernstrom, E.V., Carreiro, J.L. and Grimmelsman, K.A. (2013). "Evaluation of Economical Dynamic Exciters for Vibration Testing of Bridges." Proceedings of the 31st International Modal Analysis Conference, Garden Grove, CA.

Fernstrom, E. (2014). Global dynamic characterization and load rating of bridge structures utilizing economical dynamic excitation devices. (Unpublished Doctorate of Philosophy). University of Arkansas, Fayetteville, AR.

Fladung, W., & Brown, D. (1993). Multiple reference impact testing. *Proceedings of SPIE - the International Society for Optical Engineering, , 1923* 1221-1229.

Grimmelsman, K.A., Lindsey, J.D., Dufour, R.T. and Norris, J.T. (2014). "Excitation Related Uncertainty in Ambient Vibration Testing of Bridges." *Proceedings of the 32nd International Modal Analysis Conference*, Orlando, FL.

He, J., & Fu, Z. (Eds.). (2011). *Modal analysis* (1st ed.). Woburn, MA: Butterworth-Heinemann.

Lenett, M., Brown, D., Hunt, V., & Helmicki, A. (2000). Performing bridge condition assessment with spliced multi-reference impact data. *Proceedings of IMAC-XVIII: A Conference on sSructural Dynamics,* Westin La Cantera Resort, San Antonio, Texas. 1307-1312.

Lenett, M., Catbas, N., Hunt, V., Aktan, A. E., Helmicki, A., & Brown, D. (1997). Issues in multi-reference impact testing of steel-stringer bridges. *Proceedings of the International Modal Analysis Conference- IMAC, 1 and 2*, 374-380.

Lenett, M., Helmicki, A., & Hunt, V. (2000). Multi-reference impact testing of FRP bridge deck material. *Proceedings of SPIE, the International Society for Optical Engineering,4062*, 8-13.

Lenett, M., Hunt, V., Helmicki, A., & Brown, D. (2002). Identifying bridge behavior and condition through multi-reference impact data. *Proceedings of Imac-Xx: Structural Dynamics, 1 and2*, 1587-1591.

Liao, Y., Zhou, Y., & Qin, P. (2012). Structural identification of an old bridge by multiple reference impact test method. *Advanced Materials Research, 594*, 1132-1137.

Madhwesh, R., & Aktan, A. (1992). Flexibility by multireference impact testing for bridge diagnostics.*118*(8), 2186-2203.

Miller, R. A. (1992). Nondestructive and destructive testing of a three span skewed R. C. slab bridge. Engineering Mechanics Division of the American Society of Civil Engineers in Conjunction with the Structures Congress, , 150-161.

Patjawit, A., & Kanok-Nukulchai, W. (2005).
Health monitoring of highway bridges based on a global flexibility index *Engineering Structures, 27*, 1385-1391.

Schwarz, B., & Richardson, M. (1999, Experimental modal analysis. *CSI Reliability Week, ,* 1-12.

Stewart M.A., Manahan, M. P., McCowan, C. N., Holt, J. M., Marsh F.J., & Ruth, A. E. (2000). The history and importance of impact testing. *American Society for Testing and Materials,1380*, 3-16.

Zhang, J., & Moon, F. (2012). A new impact testing method for efficient structural flexibility identification. *Smart Materials and Structures, 21*, 1-11.